Journal of Geoscience and Environment Protection, 2024, 12, 221-251
https://www.scirp.org/journal/gep
ISSN Online: 2327-4344
ISSN Print: 2327-4336

Spatial and Temporal Variability of Solar Irradiance in Botswana

Isiah Tefo Kazapua[1,2,3], Yueyue Yu[1*], Meijia Hu[1,4], Jin Liu[5]

[1]School of Atmospheric Sciences, Key Laboratory of Meteorological Disaster of Ministry of Education, Collaborative Innovation Center on Forecast and Evaluation of Meteorological Disasters (CIC-FEMD), Nanjing University of Information Science and Technology, Nanjing, China
[2]Ministry of Environment, Natural Resources and Tourism, Gaborone, Botswana
[3]Botswana Department of Meteorological Services, Gaborone, Botswana
[4]Northwest Engineering Corporation Limited, Xi'an, China
[5]Reading Academy, Nanjing University of Information Science and Technology, Nanjing, China
Email: ttefoxx@gmail.com, *yuyy@nuist.edu.cn

How to cite this paper: Kazapua, I. T., Yu, Y., Hu, M., & Liu, J. (2024). Spatial and Temporal Variability of Solar Irradiance in Botswana. *Journal of Geoscience and Environment Protection, 12,* 221-251.
https://doi.org/10.4236/gep.2024.1211013

Received: October 24, 2024
Accepted: November 25, 2024
Published: November 28, 2024

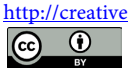

Abstract

This study evaluated the potential of Botswana's sustainable energy production using ERA5 reanalysis data of solar irradiance variability on an optimally inclined plane from 1971 to 2020. Spatial-temporal solar irradiance fluctuations were the focus of the study, and the relation to cloud cover and aerosol optical depth was investigated. The key findings suggest that the summer/rainfall season (November to March) is the peak season with average monthly solar irradiance of 313 - 445 W/m^2 across southern, central, and northern parts of Botswana, the Kalahari Desert and the Makgadikgadi Pans being identified as prime sites for solar energy projects. The long-term trend analysis showed a decrease in solar irradiance in December but a consistent increase from August to October, indicating a potential shift in solar resources toward an earlier season. Contrary to other studies that found that aerosol optical depth dominates effects on long-term trends and year-to-year variability of solar irradiance, for this case, cloud cover, particularly mid-level clouds, is found to have a more dominant role in Botswana. Solar irradiance characteristics of three distinct regions were identified through K-means clustering. Moreover, Ensemble Empirical Mode Decomposition (EEMD) analysis showed the commonality and time scale linkage between solar irradiance and cloud cover between the identified regions. These results highlight the importance of including cloud-related weather patterns under the global warming scenario in solar energy planning and emphasize the secondary role of aerosols in Botswana, thus providing critical information for the region's solar energy development and policy formulation.

Keywords

Solar Irradiance, Botswana, Cloud Cover, Photo-Voltaic Systems, K-Means Clustering, EEMD

1. Introduction

For Botswana, solar energy is a significant power source capable of sustaining numerous human activities (Okakwu et al., 2019). Given its ample sunlight and moderate temperature, the country has significant potential to rely on solar energy as a sustainable source. Despite their heavy reliance on fossil fuels, coal-fired power plants like Morupule B meet most of the nation's electricity demand (Botswana Power Corporation, 2021). Noteworthy are the significant energy problems that occurred in 2013 and early 2014, where there were frequent power interruptions, and hence emphasize the need to diversify and adopt cleaner, renewable sources. Hence, this solar energy can enable Botswana to align with a more sustainable future by reducing its carbon footprint and improving regional energy security.

Geographically positioned to get plenty of sunlight, Botswana, with its semi-arid climate and hot, dry weather for most of the year (Batisani & Yarnal, 2010), is perfect for the growth of solar energy. With an average insolation of 21 MJ/m^2 on a horizontal surface and over 3,200 hours of sunlight yearly (SKR Engineering College et al., 2017), the nation claims one of the highest solar irradiance rates worldwide. These favorable circumstances and growing attempts to support renewable energy have inspired projects aiming at using solar power for electricity generation, thereby building trust in the viability of such projects.

Photovoltaic (PV) technology, which directly converts sunlight into electricity, has emerged as a leading solution for solar irradiance utilization (Bhayo et al., 2020). The simplicity, reliability, low power, long endurance, and scalability of PV solutions are well-matched to many problems (Kalogirou, 2009; Yahyaoui et al., 2023). With technical assistance from the government, Botswana Power Corporation has already initiated programs to incorporate solar photovoltaic technologies into the country's energy system. These schemes emphasize the critical role that PV will play in Botswana's shift to a greener energy space, increased energy security, and lower carbon emissions.

An adequate understanding of the climate of solar irradiance (both temporally and physically) is required to optimize PV system design, reduce risk, and improve solar energy deployment (Mühlemann et al., 2022). Previous research on elements of solar radiation variability in Botswana has concentrated on direct solar irradiation over specific sites (Nijegorodov et al., 2005; Tlhalerwa & Mulalu, 2019). Observed during the summer/rainfall months (November to March), they discovered the maximum solar radiation values in the southwest (Kgalagadi and Ghanzi) with 291 W/m^2 followed by the center sections (Sua-pan) with 268 W/m^2 and the northern parts (Ngamiland and Chobe). Botswana's location causes

notable mean annual solar radiation; the UV component has risen over the past eight years from 1995 to 2003. Botswana also has great concentrated solar plant potential that surpasses current electricity consumption.

Several recent studies suggest via changing atmospheric circulation patterns and cloud cover the likely influence of global warming and climate change on solar irradiance (Voigt et al., 2020). Higher temperatures can significantly reduce cloud cover, enabling more solar irradiance to reach the surface of the Earth (Bright & O'Halloran, 2019). Research indicates that Botswana's rainfall has declined, and temperatures have risen since 1981, primarily due to climate change (Kenabatho et al., 2012; Byakatonda et al., 2018). Since cloud cover will decrease under drier conditions, solar irradiance might benefit from it. Lassman et al. (2020) conducted their study in Botswana and found the average concentration of particulate matter or aerosols with diameters < 2.5 microns (PM2.5) to be 9.4 $\mu g \cdot m^{-3}$. This value is below the annual limit of 10 $\mu g \cdot m^{-3}$ recommended by the World Health Organization (WHO). It is in close agreement with the estimate derived from satellite and model data used by the Global Burden of Disease (GBD), which is 9.1 $\mu g \cdot m^{-3}$. Further, they revealed that the inorganic aerosol, primarily ammonium sulfate (average 35% by mass), is a significant component of the particle phase. The aerosol also includes a substantial fraction of carbonaceous material, consisting of water-soluble organic carbon (mean of 12 % by mass) and black carbon (mean of 18% by mass), which is not inorganic sulfate. These findings were consistent with the major coal power plants situated upwind of the measuring site and the level of solid fuel combustion in their research region.

This paper demonstrates several new contributions to understanding solar irradiance in Botswana; it is the first comprehensive study that assesses solar irradiance variability varying in Botswana upon 50 years of ERA5 reanalysis data with a robust long-term view. For our best understanding of the patterns of solar irradiance, we use a spatial, temporal, and statistical strategy using EEMD and k-means clustering. We consider all the parts of solar irradiance (direct, diffuse, and reflected). This enables us to calculate the optimum solar irradiance on the inclined plane across the country to be treated as efficiently as possible with the photovoltaic surface setups. We investigate the relationship between solar irradiance variability and local influencing factors such as cloud cover and aerosols at different timescales. We offer new insights into the region's drivers of solar energy potential.

Using ERA-5 re-analysis data covering a long period from 1971 to 2020, this study elucidates the main features of solar irradiance variability in Botswana, both spatially and temporally, annually and seasonally. The results can also offer tremendous information and helpful insights into planning, forecasting, and policy formulation of solar irradiance. Section 2 describes the data analysis methodology, while Section 3 thoroughly investigates solar irradiance's spatial and temporal variability across Botswana. In the same section, we further investigate the factors affecting variability in solar irradiance: cloud cover and aerosols. Section 4 presents the conclusions.

2. Data and Methodology

2.1. Data

The climate data used in this study are estimates of land, marine, and atmosphere climate variables time-dependent at hourly through ECMWF Reanalysis v5 (ERA5), which covers the period from 1940 to the present. ERA5 spans the planet on a 31 km grid and resolves the atmosphere with 137 levels. It replaces the ERA-Interim reanalysis and offers hourly output and uncertainty estimates with a 31 km horizontal resolution (Hersbach et al., 2020; Ahamed & Alam, 2022).

The ERA5 data includes the main components needed to calculate optimal solar irradiance on an inclined plane: FDIR (direct solar irradiance at the surface), UV-visible albedo (surface albedo for direct irradiance), and SSRD (surface solar irradiance downwards) (Hogan, 2015).

Botswana's observational data availability was limited, as only the direct UV component known as the SSRD was available for a short period of 1983 to 2015; thus, to compute the optimal total solar irradiance on an inclined plane, all three components: direct, diffuse, and reflected solar radiation were needed. However, a thorough comparison between SSRD from Botswana station data and SSRD from ERA5 showed high correlation coefficients of about 0.95 at a 95% significance level obtained by the student's t-test; they continuously showed similar trends, validating ERA5's suitability in the absence of observational data. Standardized anomalies in **Figure 1(b)** illustrate the high consistency between SSRD Botswana observational data and SSRD ERA5 reanalysis data.

A thorough comparison analysis of the two datasets included in the Supplementary material section showed that both BW Data and ERA5 SSRD have peaks in solar radiation during their summer for December, January, and February, and BW Data comes in at 282 W/m^2 during summer. However, between December and February, radiation levels are at a high, surpassing 300 W/m^2 during the summer, while in winter months (May to July), the levels reach their lowest point of below 200 W/m^2 in June and July. Heightened attention is also paid to the disparity between ERA5 SSRD and BW Data values, particularly in winter, which might be attributed to methodological differences or spatial resolution. Standard deviation analysis found higher standard deviations in summer (over 25 W/m^2) and higher direct solar radiation component variability, compared with winter months (below 10 W/m^2) when standard deviation values are minor and imply more stable conditions for daylight levels. A strong positive correlation (0.87 to 0.98) between the datasets from month to month implies similar longer-term trends and seasonal patterns. Southern stations receive more solar radiation than northern ones, with both datasets exhibiting an overall agreement in the spatial patterns but with some magnitude differences in summer. In addition, we observe higher variability in the summer months (mean 25 - 32 W/m^2, standard deviation) in southern regions and lower variability in winter (6 - 15 W/m^2). In some areas of the region, ERA5 SSRD may have slightly higher standard deviations, perhaps reflecting greater-scale atmospheric processes that local measurements may not

fully represent.

Additionally, monthly cloud cover data (total, high, medium, and low clouds) derived from 24 hourly ERA5 and aerosol data derived from CAMS global reanalysis (EAC4) reanalysis data with horizontal resolutions of 0.25˚ × 0.25˚ and 0.75˚ × 0.75˚ were used to analyze their relationship to solar irradiance in Botswana from 1971 to 2020 and 2003 to 2020, respectively.

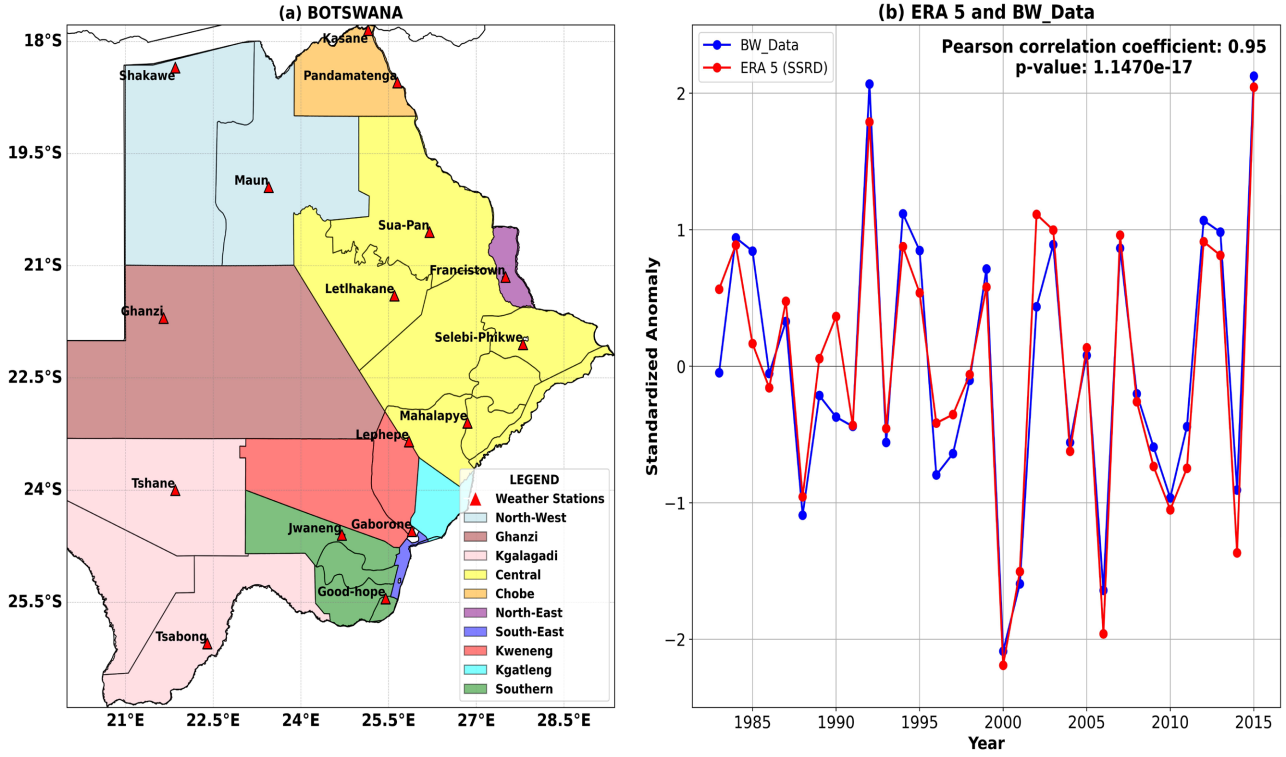

Figure 1. (a) The Botswana map shows the distribution of districts and observational stations; (b) Standardized annual mean direct solar irradiance at the surface anomalies averaged over all stations/grids of Botswana derived from the Botswana observational station data and ERA5 Reanalysis data, respectively. Also, the Pearson correlation coefficient and statistical significance were denoted at a 95% confidence interval.

2.2. Methodology

2.2.1. Total Solar Irradiance Calculation on a Tilted Surface—The Case of a Photovoltaic (PV) System

Thus, the hourly irradiance on an inclined collector surface has to be designed, and performance must be calculated based on observations or predictions of solar irradiance on a horizontal surface (Shekata et al., 2024). The most readily accessible statistics often provide total irradiance over hours or days on a horizontal surface, but what is required is direct, diffuse, and reflected irradiance on the plane of collection. To be used in solar process design techniques, the monthly average daily irradiance on the tilted surface must be calculated using the equation provided by (Sarbu & Sebarchievici, 2017).

$$I_{T,\Sigma} = R_D I_D + \frac{1}{2}(1+\cos\Sigma) I_d + \frac{1}{2}(1-\cos\Sigma)\rho_g I_T \quad (1)$$

$$I_D = I_{DN}\cos\theta \tag{2}$$

$$I_{DN} = A_0 e^{-B/\sin\beta} \tag{3}$$

I_{DN} represents the direct average irradiance calculated by using Equation (3). A_0 represents the extra-terrestrial irradiance at air mass $m = 0$; B is the atmospheric extinction coefficient; β is the sun's altitude over the horizon in degrees (Stephenson, 1967). The geometric factor R_D represents the ratio of direct irradiance on a slanted plane in comparison to a horizontal surface at any given time and is $I_{D,\Sigma}/I_D$ given by:

$$R_D = \frac{I_{D,\Sigma}}{I_D} = \frac{I_{DN}\cos\theta}{I_{DN}\cos\theta_z} = \frac{\cos\theta}{\cos\theta_z} \tag{4}$$

Equations that connect the angle of incidence θ of direct irradiance on a surface with other angles are presented by (Duffie & Beckman, 2013);

$$\begin{aligned}\cos\theta = {} & \sin\delta\sin\varphi\cos\Sigma - \sin\delta\cos\varphi\sin\Sigma\cos\psi + \cos\delta\cos\varphi\cos\Sigma\cos\omega \\ & + \cos\delta\sin\varphi\sin\Sigma\cos\psi\cos\omega + \cos\delta\sin\Sigma\sin\psi\sin\omega\end{aligned} \tag{5}$$

$$\cos\theta = \cos\theta_z\cos\Sigma + \sin\theta_z\sin\Sigma\cos(\phi - \psi) \tag{6}$$

Duffie and Beckman estimated the R_D based on the angle difference φ-Σ and latitude φ, and its values were provided in their publication (Duffie & Beckman, 2013). Given a specific ratio R_D, the direct sun irradiance on a tilted surface can be calculated using Equation (4).

$$I_{D,\Sigma} = R_D I_D \tag{7}$$

To calculate total solar irradiance $I_{T,\Sigma}$, the direct irradiance, diffuse irradiance components, and ground-reflected irradiance are summed up. The isotropic diffuse representation of the sky, initially suggested by Liu and Jordan (1960) and later expanded by Klein (1977), is then utilized to assess both diffuse irradiance and ground-reflected irradiance. The diffuse irradiance on the tilted surface $I_{d,\Sigma}$ is defined by

$$I_{d,\Sigma} = \frac{1}{2}(1+\cos\Sigma)I_d \tag{8}$$

where I_d is the scattered/diffuse irradiance on a surface oriented horizontally. The formula for the irradiance reflected from the ground on the slanted surface $I_{r,\Sigma}$ is provided by

$$I_{r,\Sigma} = \frac{1}{2}(1-\cos\Sigma)\rho_g I_T \tag{9}$$

where ρ_g denotes the diffuse reflectance of the ground (Bostan et al., 2011) and I_T is the total solar irradiance on a surface oriented horizontally. The total solar irradiance on the surface tilted at a certain angle is combined into three components.

$$I_{T,\Sigma} = R_D I_D + \frac{1}{2}(1+\cos\Sigma)I_d + \frac{1}{2}(1-\cos\Sigma)\rho_g I_T \tag{10}$$

Utilizing ERA5 datasets, I_D = direct solar radiation at the surface, denoted by

the short name FDIR; I_T = surface solar radiation downwards, denoted by the short name SSRD; and UV-visible surface albedo for direct radiation, is denoted by ALUVP. In addition, I_d = diffuse/scatter radiation results from subtracting FDIR from SSRD.

In the later section, solar irradiance (SIR) refers to the total irradiance on the tilted surface with the optimal solar panel tilt angle. The optimal tilt angle used was −29˚ for PV systems facing north (Jacobson & Jadhav, 2018). Monthly averages were then produced from 1971 to 2020. The standard deviation (SD) was calculated to evaluate yearly variations in solar irradiance (Streiner, 1996).

2.2.2. Trend Analysis

Trend direction was determined using the Mann-Kendall (MK) non-parametric test (Mann, 1945; Kendall, 1975). The MK test is commonly used statistically in hydrological time series analysis to test the significance of a trend (Yue & Wang, 2004). This is intuitive and stable when data is not normally distributed and can handle outliers and missing data (Ndabagenga et al., 2023). The Z value and the p-value from the MK test are standardized statistics according to the methodology of Yue and Wang (2004). Trends passing with positive Z values ascend, and trends passing with negative values descend. If a trend is below 0.05 in a p-value, it is statistically significant. Sen's (1968) nonparametric technique was used to determine the amplitude of the trend in the time series.

2.2.3. K-Means Clustering Analysis

Spatial patterns and locations with similar solar irradiance were identified with K-means cluster analysis. Edwards et al. (1965) analyze variance where the data points are split into compact clusters, and the process is repeated until the hierarchical "tree" diagram is reached. The obtained elbow and silhouette score methods were applied to determine the best number of clusters (Umargono et al., 2020; Shahapure & Nicholas, 2020). This process was used to segment Botswana's regions regarding solar irradiance distribution from 1971 to 2020 with identical solar irradiance characteristics.

2.2.4. Ensemble Empirical Mode Decomposition (EEMD)

The EEMD method is a highly flexible and practical data analysis methodology for analyzing nonlinear and nonstationary data. Hilbert transforms (Huang et al., 1998) can be applied to decompose complex datasets into several intrinsic mode functions (IMFs); accomplishing this was the motivation for using this approach. A filtering algorithm was used to derive the intrinsic mode functions (IMFs) to reconstitute the sub-signal, which contains various attributes of the original signal at different temporal scales. We then obtain a new residual signal close to a monotonic signal coming from the fundamental trend of the original signal (Gaci, 2016).

EEMD helps process solar irradiance data, which is often nonlinear and non-stationary. It maintains critical salient features and reduces noise by omitting

measurement errors and atmospheric noise. EEMD allows for identifying the dominant modes of variability in the solar irradiance signal and, thus, primary oscillatory patterns. Additionally, it offers time-frequency localization, enabling the identification of transient events and localized changes in solar irradiance intensity.

3. Results and Discussion

Displayed in **Figure 2** is the time series of yearly mean solar irradiance averaged over all grid points of Botswana derived from ERA5 Reanalysis data during the past 50 years since 1971. It is seen that the mean irradiance value over the 50 years was 270.79 W/m^2. The peak solar irradiance occurred in 2015, while the lowest was recorded in 2000. Similar to the findings of Ma et al. (2013), the yearly average trend shows a moderate and continuous increase in solar irradiance from 1971 to 2020. However, The Mann-Kendall test yielded an insignificant p-value of 0.806, indicating a slight positive slope of 0.0163 (W/m^2)/year, suggesting no significant upward trend in the yearly mean solar irradiance averaged over Botswana over the study period.

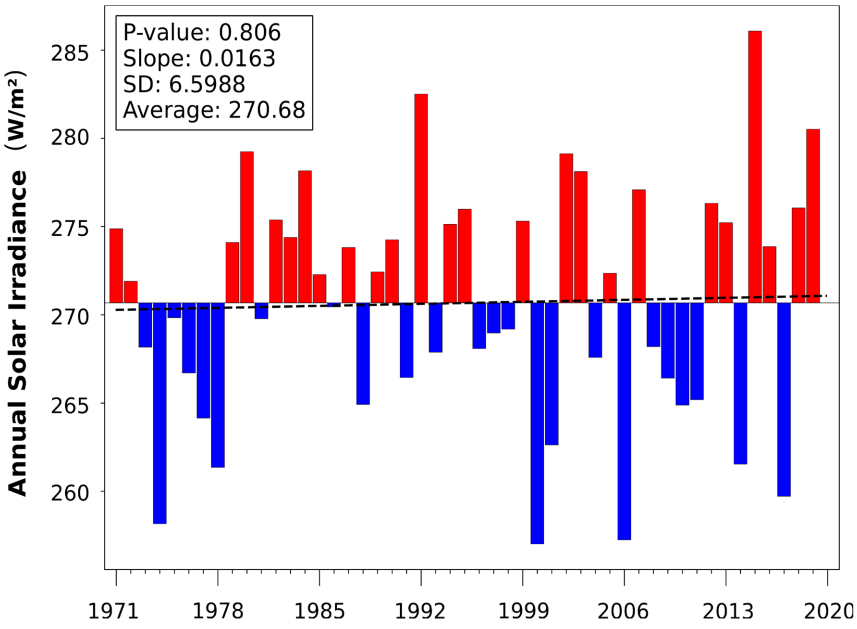

Figure 2. Time series of annual solar irradiance trend (W/m^2) in Botswana (1971-2020).

According to previous studies, though Botswana has hot and dry weather for most of the year (Batisani & Yarnal, 2010), it still has a summer/rainfall season from November to March and winter months from May to July (Batisani & Yarnal, 2010; Byakatonda et al., 2018). **Figure 3** illustrates the seasonal march of the climatological means and the monthly standard deviations of solar irradiance from January to December in Botswana. As seen from **Figure 3(a)**, solar irradiance values ranged between 161.08 and 373.87 W/m^2. They exhibited solar

irradiance values above climatology from September to March, corresponding to Botswana's summer/rainfall seasons (Batisani & Yarnal, 2010; Byakatonda et al., 2018). Peak values of December solar irradiance were recorded at 373.87 W/m^2. The values observed were below climatology in April, May, June, July, and August. Additionally, June had the lowest solar irradiance values of 161.08 W/m^2. Furthermore, **Figure 3(b)** highlights the standard deviation of solar irradiance for each month, given a mean value of 18.03 W/m^2 and values from 5.09 to 39.66 W/m^2. Standard deviation values change seasonally, from higher summer values (November-March) to lower winter and spring values (April-August), like seasonally varying climatological mean. However, it is noticeable that the standard deviation values are higher for January and February among the summer months, even though their climatological mean is lower than November and December. This indicates the more significant solar irradiance variability; thus, particular attention should be paid to its prediction from January to February.

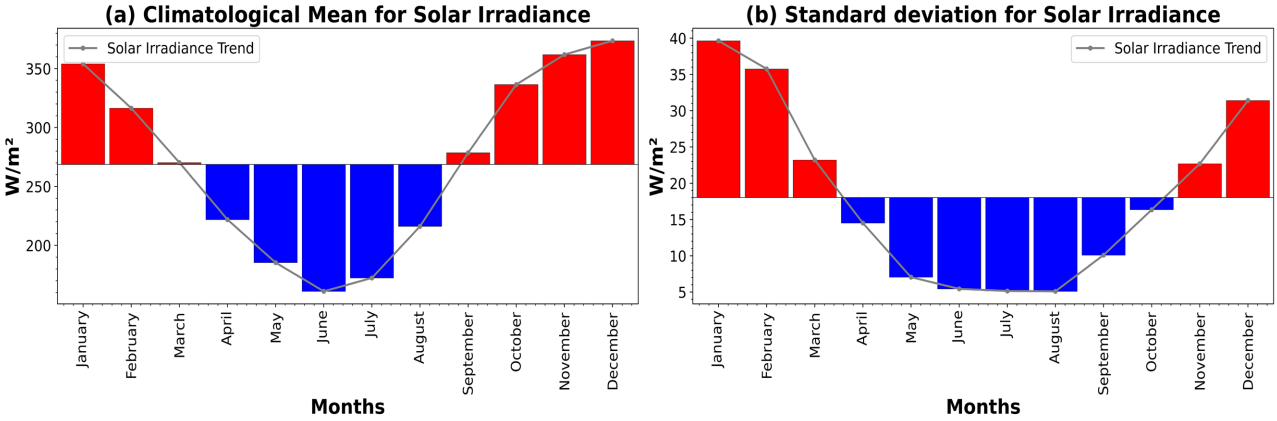

Figure 3. (a) Climatological mean and (b) standard deviation of monthly solar irradiance in W/m^2 averaged over Botswana (1971-2020).

An inspection of the time series of solar irradiance in each month (**Figure 4**) yields that in December (**Figure 4(l)**), when solar irradiance reached its maximum value, a sharp decreasing trend was observed with a slope of −0.5404 and a statistically significant Mann-Kendall p-value of 0.047. On the other hand, **Figure 4(h)-(j)** show solar irradiance in August, September, and October (ASO), which is characterized by a sharp increasing trend. Successfully performed Mann-Kendall tests yielded statistically significant p-values of 0.021, 0.002, and 0.003, way above chance. Above solar irradiance in ASO has predominately been above climatology in the most recent period following 2007. Moreover, after 2007, the values of October are around 340 to 350 W/m^2, and even more significant than those in November and December. The trend analyses of monthly solar irradiance in Botswana indicate a possible shift in the season of high solar irradiance, showing a tendency toward earlier arrival of ample solar irradiance during the spring months. For the other months, no trends were seen.

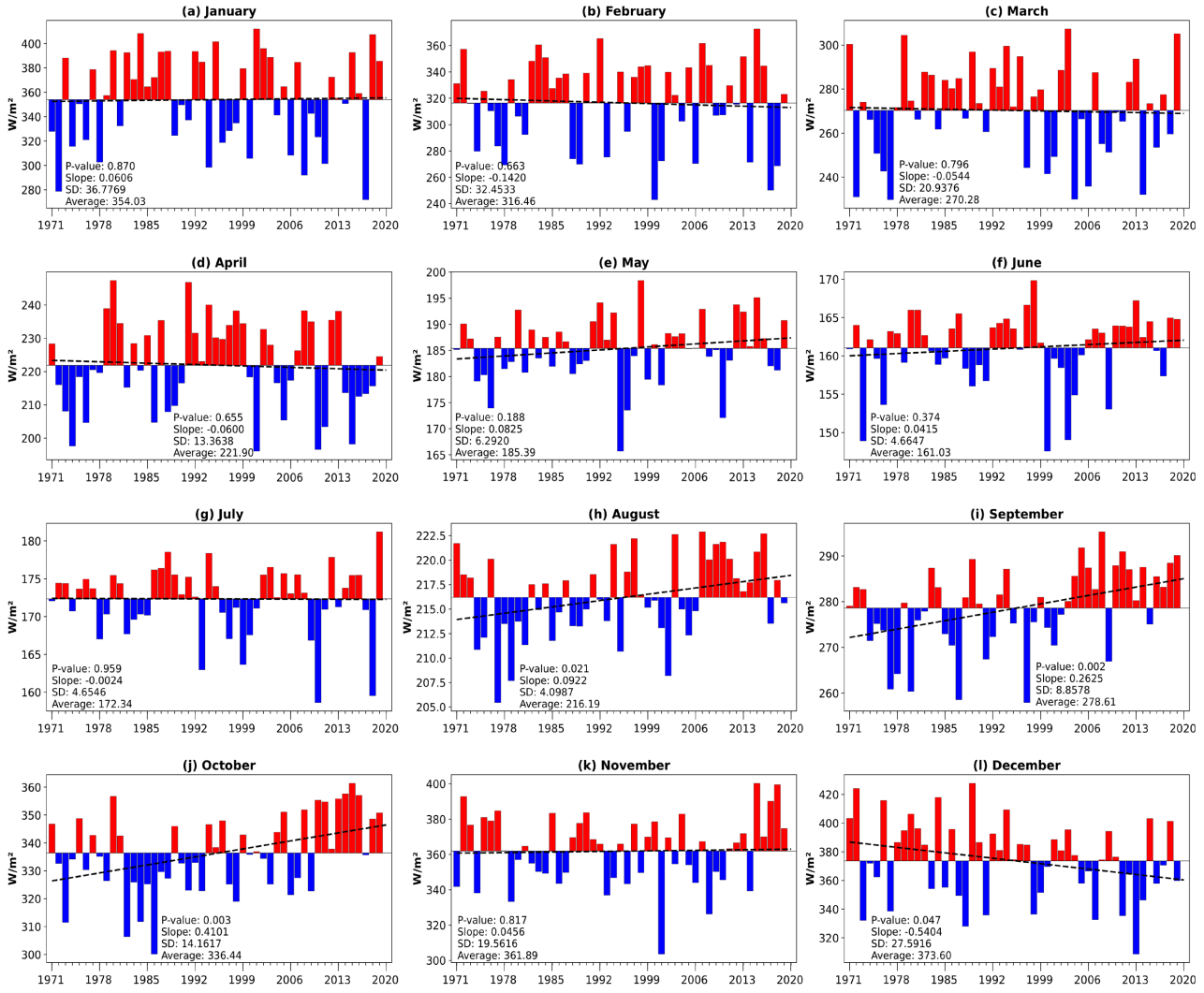

Figure 4. (a)-(l) Time series of the monthly solar irradiance in Botswana (W/m^2) from 1971 to 2020 and the linearly fitted line. The linear trend slope, corresponding P-value for statistical significance at a 95% confidence interval, climatological average value (Average), and yearly standard deviation (SD) are shown in the bottom-left corner.

3.1. Spatial Distribution

Our research has revealed fascinating seasonal variations in solar irradiance. In the summer months from October to February, the entire country experienced maximum solar irradiance, with values ranging from 313 to 445 W/m^2 (**Figure 5(a)**, **Figure 5(b)**, **Figure 5(j)**, **Figure 5(k)**, and **Figure 5(l)**). Solar irradiance peak was observed in December with a range of 344 to 445 W/m^2 and the highest values at the southwestern part of the Kalahari Desert, 445 W/m^2. The pattern of spatial solar irradiance falling from southwest to northeast in other months, such as October, November, January, and February, is also evident. This is consistent with the spatial pattern of direct solar irradiance, as Nijegorodov et al. (2005) and Tlhalerwa and Mulalu (2019) reported. In March (**Figure 5(c)**), solar irradiance dropped to values around 280 W/m^2 from the previous month of February, while the spatial pattern remains (**Figure 5(b)**). In the winter months from May to July

(Figure 5(e)-(g)), decreased levels of solar irradiance were recorded across the entire research region. June displayed the minimum solar irradiance value of 148 W/m^2 in the south and southeast regions (Figure 5(f)). August and September (Figure 5(h)-(i)) show a noticeable and region-uniform rise in solar irradiance, with values reaching 247 W/m^2 and 285 W/m^2, respectively. However, the east-most corner that covers the Northeast and Southcentral districts seems to increase more slowly.

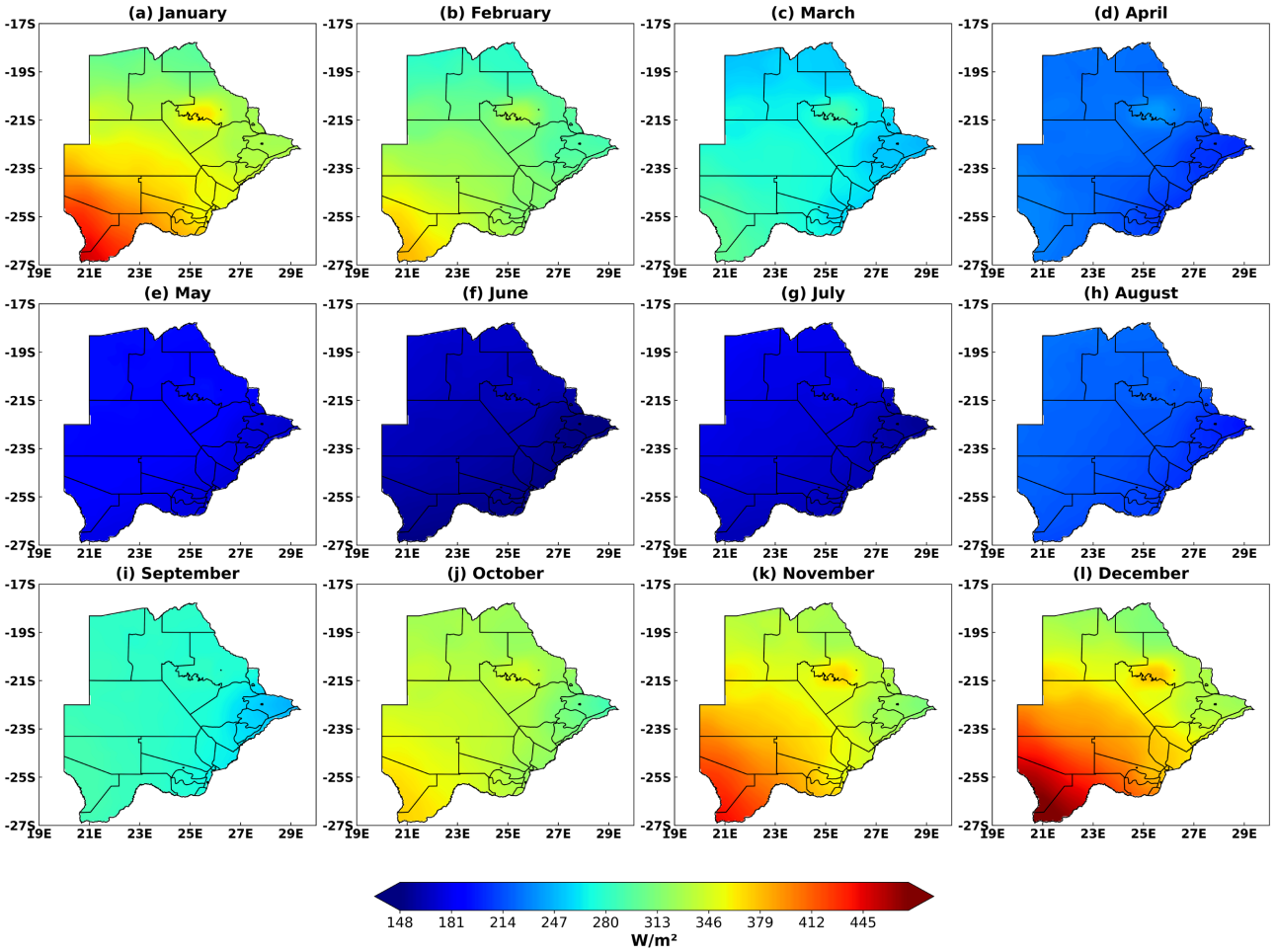

Figure 5. (a)-(l) Maps of climatological mean solar irradiance (W/m^2) in Botswana (1971-2020).

Our research has uncovered a crucial aspect of solar irradiance: the impact of water levels on the visibility of the hotspot. A single overriding characteristic in most spatial maps was the hotspot, mainly over the Makgadikgadi Pans, a country-wide focal point for brine production. From January to April, this phenomenon was visible (Figure 5(a)-(d)) for solar irradiance from 247 to 360 W/m^2. In addition, in November and December (Figure 5(k) and Figure 5(l), solar irradiance is 350 and 380 W/m^2, respectively, and the same solar irradiance was observed in the hotspot. During the period from May to October (Figure 5(e)-(j)), however, the pan was filled with water obscuring the hotspot. According to

Eckardt et al. (2008), plots from November, December, January, February, March, and April show evident signs of drying up, exposing salt deposits that result in significant scattering and reflected solar irradiance. The Makgadikgadi pans are replenished by the Boteti River, fed by the Okavango Delta, with water typically reaching and filling the pans in late April, reducing the albedo of the exposed salts. Consequently, the hotspot is not visible from May to October due to reduced scattering and reflection of solar irradiance in this region.

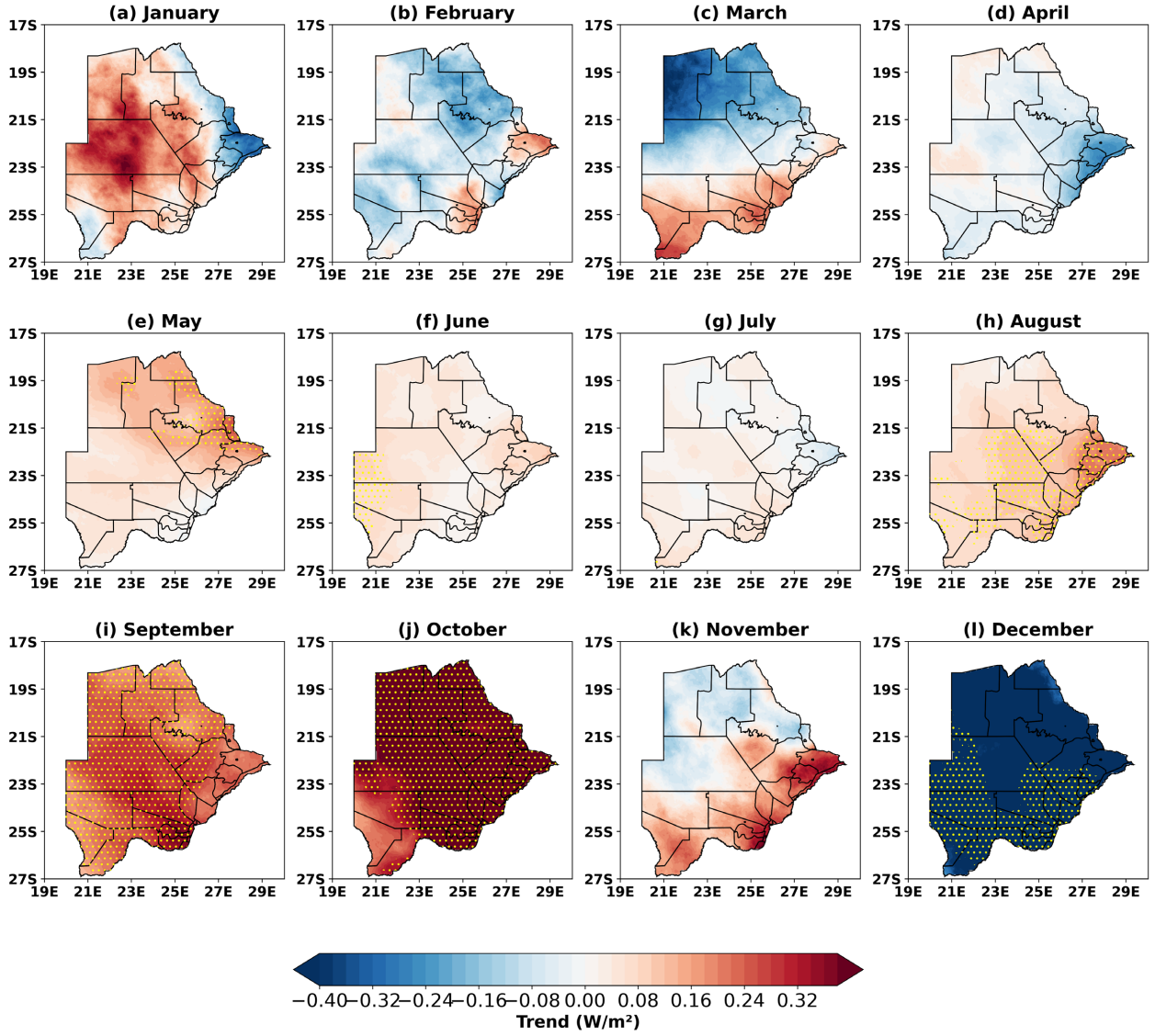

Figure 6. (a)-(l) Maps of spatial trends from 1971 to 2020 of the monthly solar irradiance in Botswana (W/m^2 per year). The dotted area indicates the linear trend above the 95% statistical significance level.

Next, we examine the spatial distribution of the linear solar irradiance trend. Figure 6 shows a statistically significant upward trend in solar irradiance over Botswana in September and October. The results of this finding could be significant in the studies about climate and environment. As with the solar irradiance in

August for the southern half (Ghanzi, Kgalagadi, Southern, Southeast, Kgatleng, Kweneng, Northeast, and Central districts), maximum irradiance also occurs in the eastmost corner. The upward trend values ranged from 0.08 to 0.32 W/m^2 per year. Conversely, in December (**Figure 6(l)**), the most pronounced downward trend was exhibited in the country's southern half, with values of −0.40 W/m^2 per year. These results echo Mucomole et al. (2023), who discovered significantly degraded solar irradiance. In addition, **Figure 6(e)** and **Figure 6(f)** also indicate a statistically significant solar irradiance increment (with statistically significant certainty) in May and June in the northeastern part of the country, as well as a tiny but statistically significant increment in the solar irradiance in Southwest during the last 50 years. This grid-scale trend analysis provides valuable insights into the temporal trends of solar irradiance across different regions of the country under the background of global warming.

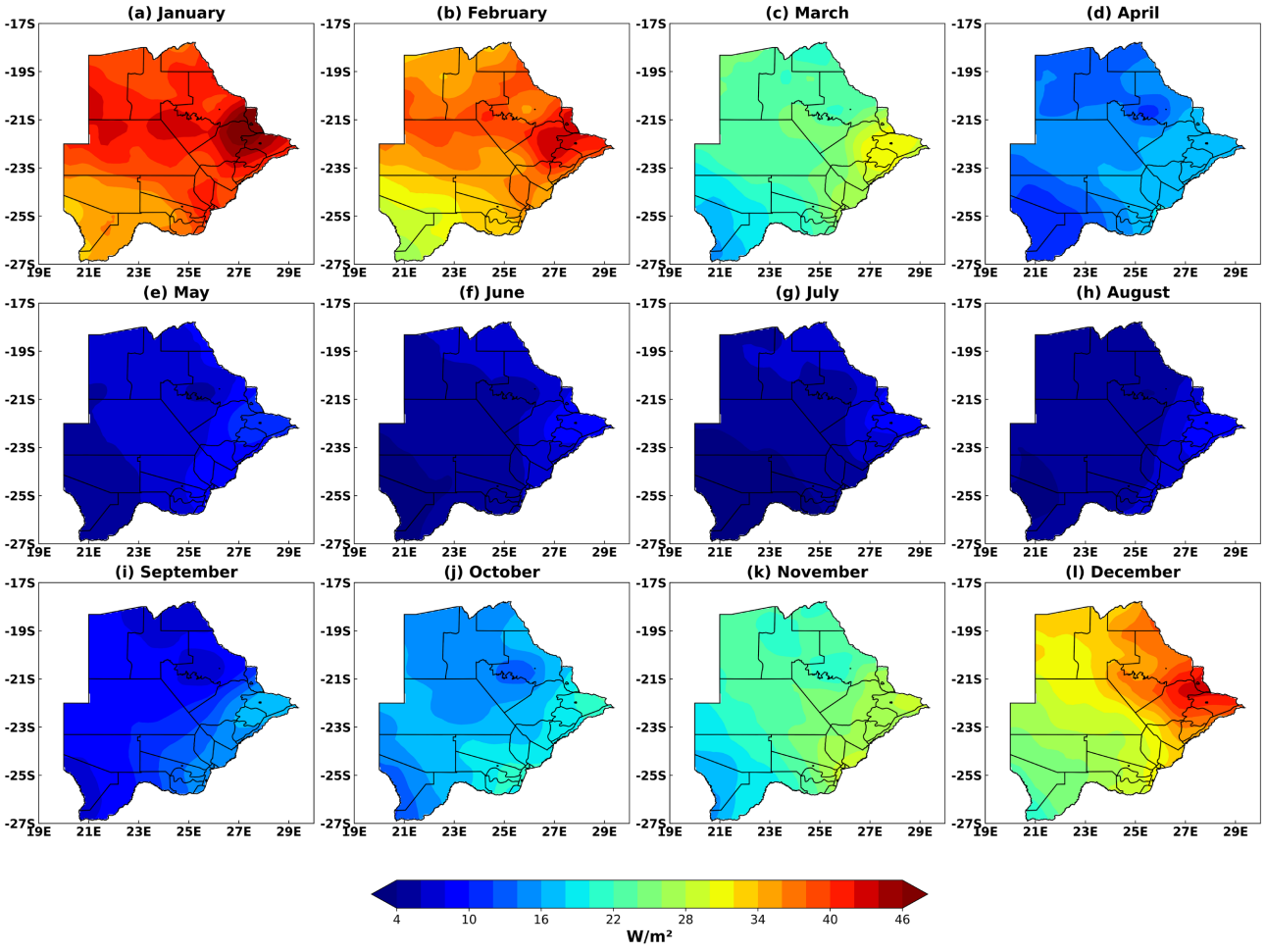

Figure 7. (a)-(l) Maps of the standard deviation of the monthly solar irradiance (W/m^2) in Botswana (1971-2020).

The spatial distribution of the yearly standard deviation of solar irradiance in Botswana is displayed in **Figure 7**. December, January, and February (**Figure 7(l)**, **Figure 7(a)** and **Figure 7(b)**) exhibited higher values of standard deviation,

varying from 24 to 44 W/m^2. In January (**Figure 7(a)**), the most significant fluctuation in solar irradiance was observed, consistent with **Figure 3(b)**; values are comparatively lower across the Kalahari Desert than in other places within the study area. In December and February, the standard deviations also increased from the southwest to the northeast (**Figure 7(l)** and **Figure 7(b)**). Comparing the spatial distribution of standard deviation (**Figure 7**) with that of the climatological mean (**Figure 5**) in these three summer months (December-February), we see that the southwest is characterized by larger values of climatological mean but smaller values of standard deviation, while the opposite is seen in the Northeast. This suggests lower/higher year-to-year variability in the Southwest/Northeast despite relatively larger/smaller averages.

During the months from April to October (**Figure 7(d)-(j)**), low levels of variability were observed, particularly across the majority of regions within the research area, with values ranging from 4.0 to 24 W/m^2. The months of June, July, and August exhibited the lowest variation values of standard deviations in solar irradiance across the entire country (**Figure 7(f)-(h)**).

3.2. Local Influencing Factors

Aerosols that cool have been found to have intense temperature, precipitation, and cloud impacts, thus altering solar energy (Levy et al., 2013; Takemura et al., 2005), which previous studies have suggested. This section will investigate the months with significant upward/downward trends of solar irradiance (August-October) and December-February months with large standard deviations of solar irradiance. This paper aims to study the linkage between the spatial-temporal cloud changes and AOD. These factors change Botswana's solar irradiance, leading to a better understanding of the factors that would eventually control the region's solar energy generation.

We first examine the climatological means and trends of Total Cloud Cover (TCC) from 1971 to 2020 in the study area, as displayed in **Figure 8(a)-(d)**. It is seen that the TCC is characterized by a decreasing trend in September and October but a significant increasing trend in December, which is noted in most Botswana regions. The regions with a significant decreasing/increasing trend of TCC correspond well to those with the maximum increasing/decreasing trend of solar irradiance. This confirms the conclusion drawn by Mucomole et al. (2023), who focused on the variability in solar irradiance in neighboring Mozambique, a country with similar climatic conditions to Botswana. Cloud coverage plays an important role; lesser cloud coverage contributes to more solar irradiance and vice versa. This is consistent with the cloud screening (albedo) effect (Pfister et al., 2003; Calbo et al., 2005).

It is generally true that the low, thick clouds primarily reflect solar irradiance and cool the surface of the Earth, while the high, thin clouds primarily transmit incoming solar irradiance. For clouds at different levels may have distinct radiative effects, we consider three types of clouds, where each type of cloud is formed

in a layer at a different level: High-Level Clouds (HLC), Medium-Level Clouds (MLC), and Low-Level Clouds (LLC). As illustrated in Figure 8(e)-(p). Figure 8(a)-(d) showed that for September and October, there was a significant reduction in total cloud cover (TCC) at 95% statistical significance over almost the entire country, which consequently led to an increase in solar irradiance. Conversely, in December, the increase in clouds country-wide led to a significant reduction in solar irradiance at a 95% significance level. Figure 9 further validates that clouds are a dominant factor in modulating solar irradiance received at the surface, as the correlations were as high as -0.96 at a 95% significant level for December, January, and February, where Botswana had the highest values of standard deviation as was noted in Figure 7(a), Figure 7(b) and Figure 7(l) for solar irradiance.

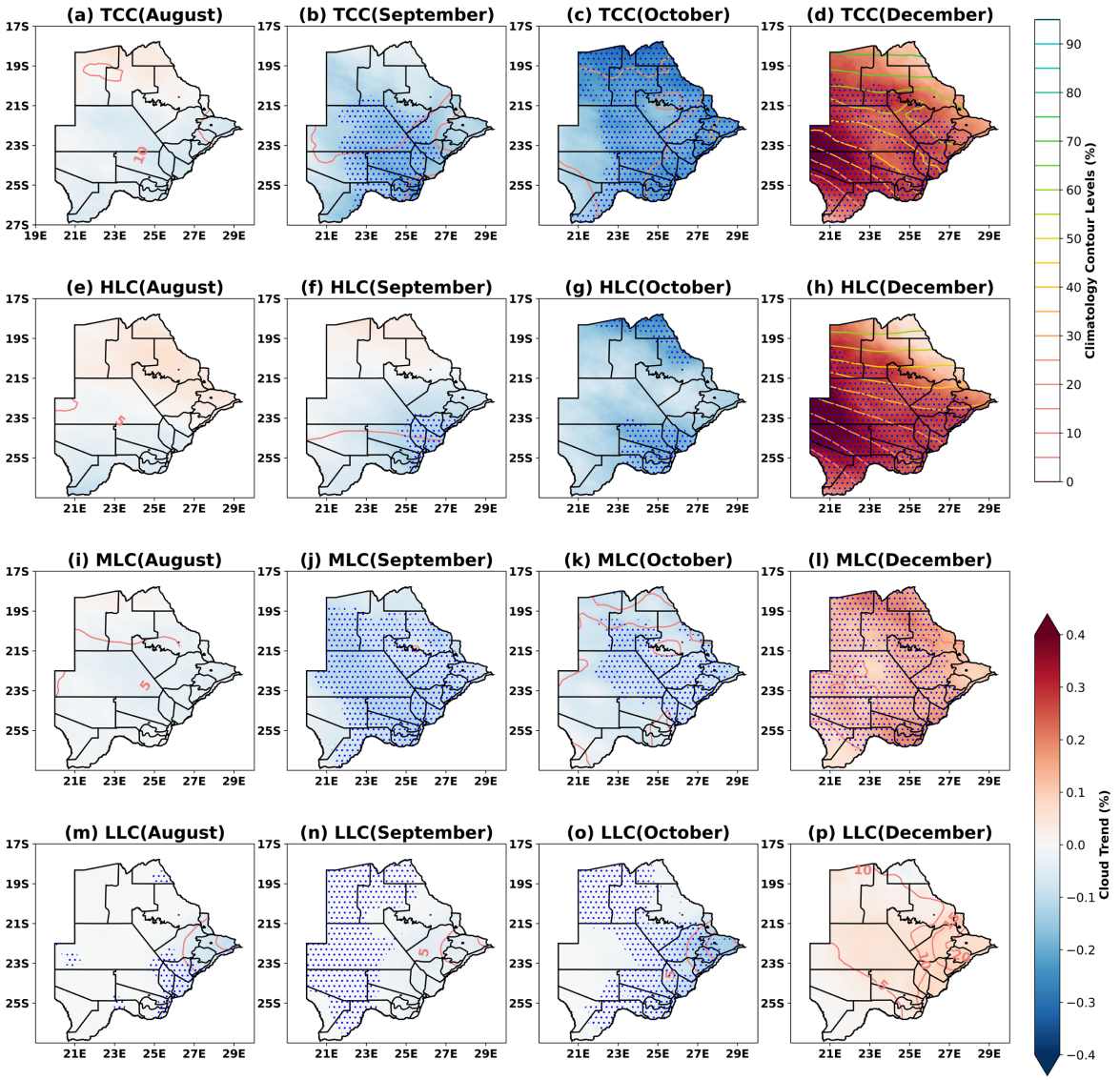

Figure 8. (a)-(p) Maps of the climatological mean (contours, %:) and linear trend (shadings, %:) different levels of cloud cover for Botswana (1971-2020). The dotted areas show statistical significance at a 95% confidence interval.

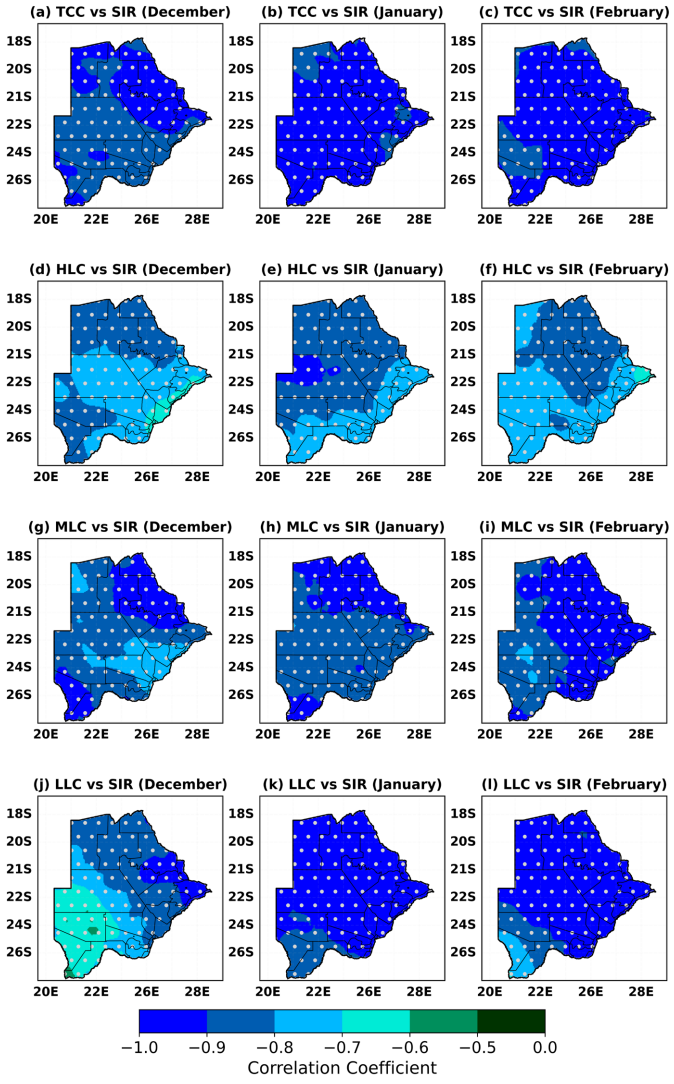

Figure 9. Monthly correlation between the TCC, HLC, MLC, and SIR in Botswana (1971-2020). The dotted areas show statistical significance at a 95% confidence interval.

Besides clouds, aerosols can directly modify the Earth's radiative balance through the backscattering and absorption of shortwave (solar) irradiance and indirectly by influencing cloud properties and lifetimes (Charlson et al., 1992; Ramanathan et al., 2001; Liu et al., 2014). Next, we examined the correlation between total aerosol optical depth and solar irradiance in **Figure 10**. Globally speaking, the values of AOD are relatively low, as with most countries in the Southern African Development Committee (SADC) region. Correlation coefficients of about −0.6 at a 95% significant level between AOD and SIR are noted in January, March, April, June, August, November, and December over the study area's Northern, Eastern, and Southern parts. However, the absolute value of correlations is mostly smaller than those between solar irradiance and cloud cover, suggesting the secondary role of aerosol in changing solar irradiance. The results for the Northern and Southern parts could be because of the water bodies in the upper Northern

parts of the country (Okavango delta, Makgadikgadi pans, Chobe river) as compared to the drier Southern parts of the country, which has the Kalahari desert. Their study (Fu et al., 2022) showed that specific humidity dominates in humid environments because aerosol particles absorb water and grow in size, increasing their optical depth. Thus, higher humidity is associated with higher AOD values relative to $PM_{2.5}$ concentrations. The results obtained over the Eastern half of the country align with the study conducted by Lassman et al. (2020) for the town of Palapye, located in the Southcentral parts of Botswana, which showed that the more dominant aerosols are sulfates and black carbon as the area inhabits the coal power plants used to generate the country's electricity. Thus, the regular burning of fossil fuels possibly constitutes these aerosols in the atmosphere. Although there is limited aerosol data for the SADC region, the results are consistent with aerosols' radiative effects, indicating that aerosols have also been an influencing factor in solar irradiance in Botswana. However, more investigation into these aerosols is required.

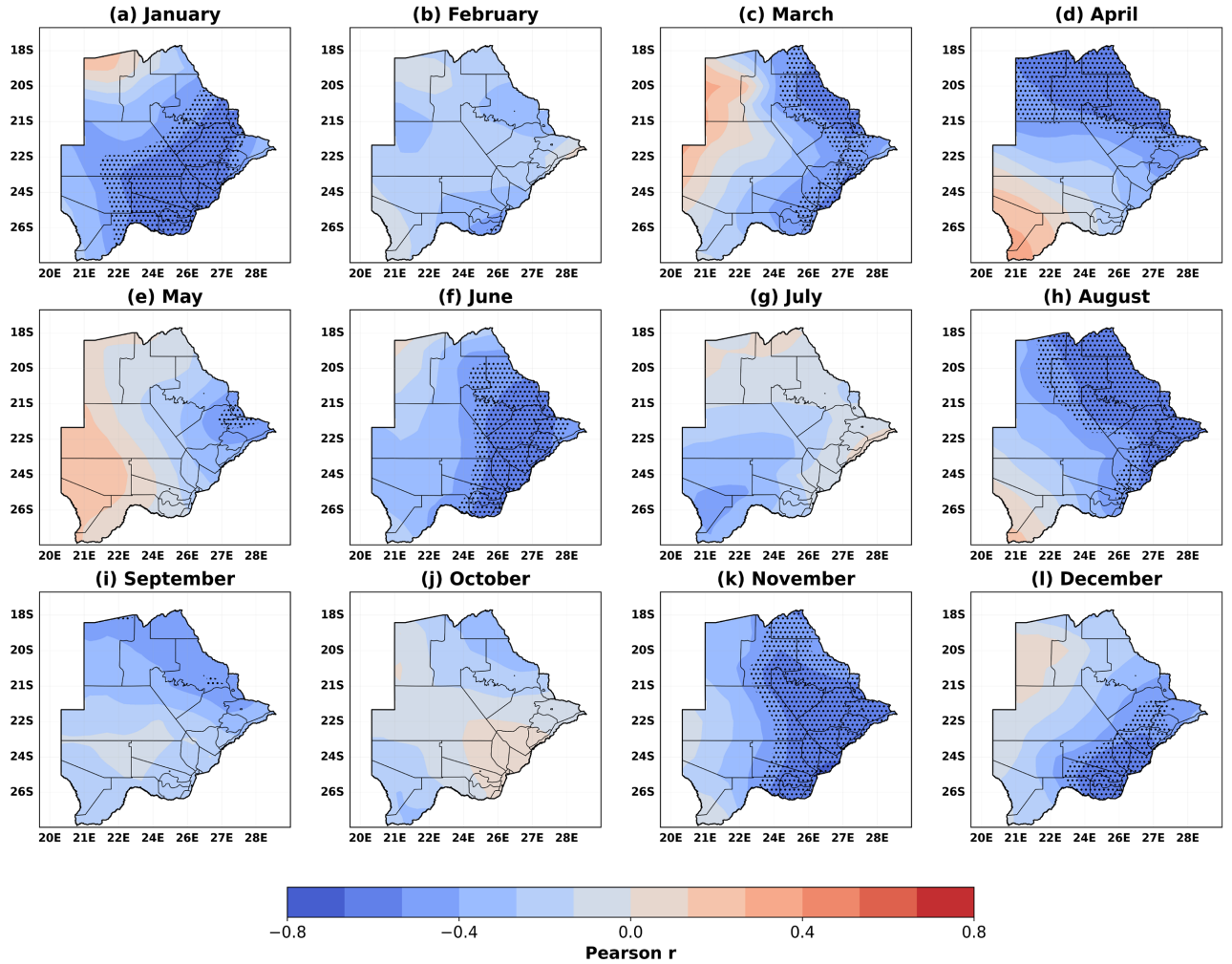

Figure 10. Monthly correlation between the Total aerosol optical depth (AOD) at 550nm and SIR for 2003-2020 in Botswana. The dotted areas show statistical significance at a 95% confidence interval.

We further calculated the correlation coefficients for different aerosols with solar irradiance in Botswana, as shown in Figure 11. The results showed that total aerosol depth (AOD 550), sulfate aerosol optical depth (SUAOD 550), dust aerosol (DUAOD 550), and black carbon aerosol (BCAOD 550), all at 550nm, are possible influencing factors, as their correlation coefficients are between −0.4 and −0.6 at a 95% confidence interval. The negative correlation is most substantial between solar irradiance and sulfate aerosol optical depth in winter or dry seasons from June to September, indicating the increasing role of sulfate aerosol in changing the solar irradiance from rain to dry seasons.

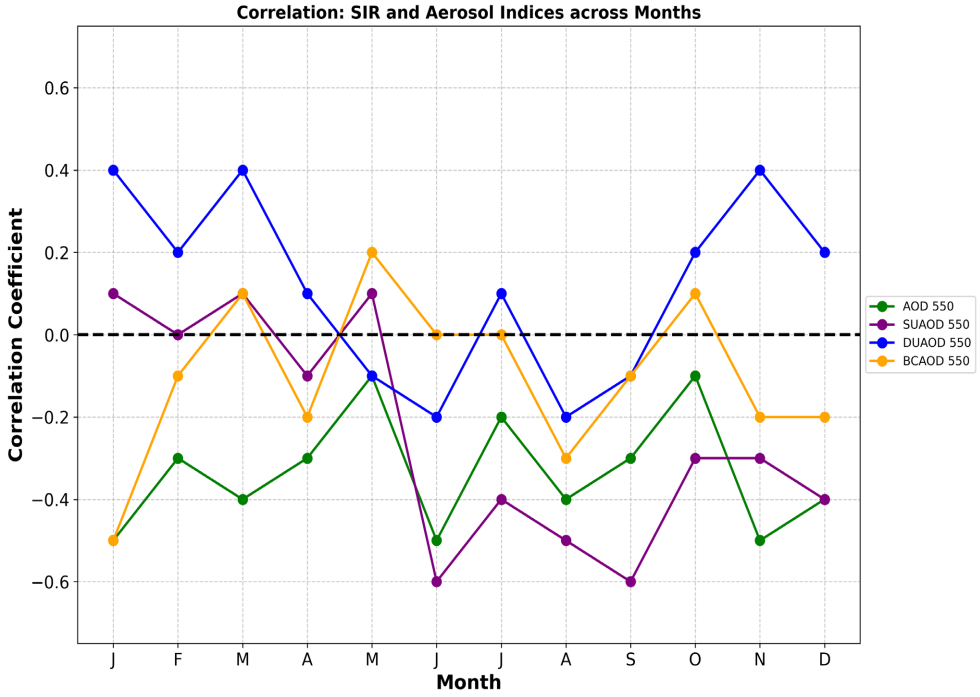

Figure 11. Monthly correlation coefficients between the Total aerosol optical depth (AOD) at 550 nm, sulfates aerosol optical depth (SUAOD) at 550 nm, dust aerosol optical depth (DUAOD) at 550 nm, black carbon aerosol optical depth (BCAOD) at 550 nm, and SIR for 2003-2020 in Botswana.

3.3. Spatial-Temporal Decomposed Changes in Solar Irradiance for the Spring Season (ASO) and Relationships with Clouds and Aerosols

Particular attention is paid to the spring months (ASO) because this is the only season with a consistent upward trend in solar irradiance. The K-means clustering method, an approach similar to that used by Umargono et al. (2020), combined with the elbow and silhouette scores method (Bansal et al., 2019), is used to divide the country into clusters, highlighting the region-dependent characteristics of solar irradiance within the country. Figure 12(a) and Figure 12(b) show that the optimal number of clusters is three (3). The distribution of three clusters for further analysis is illustrated in Figure 12(c). In particular, region one, represented by cluster 0, corresponds to the Southern region, which consists of Kgalagadi and

Southeast districts. Both districts have relatively similar average elevations: the Kgalagadi District has an average elevation of 1061 meters, while the South-East District has an average elevation of 1162 meters. Kgalagadi is the location of the infamous Kalahari desert, characterized by dunes and short shrubs. Region 2, including the Chobe and Ngamiland districts, corresponds to the northern parts denoted by cluster 1. In Ngamiland, the Okavango Delta creates a unique wetland environment with swamps and floodplains. The Chobe River forms part of the northern border of the Chobe District. Thus, the most significant water bodies are located in this region. Lastly, region 3 corresponds to Botswana's Central region, denoted by cluster 2. It includes the Ghanzi and Central districts. The landscape in Ghanzi District is predominantly flat and sandy. The Kalahari Desert extends from here, and a semi-arid environment primarily covers the region. The vegetation consists mainly of grass and thorn savannah. Transitioning to the central parts, the savannah ecosystem persists but with a greater variety of vegetation and a more pronounced presence of tall grasses, bushes, and trees than Ghanzi. Thus, there is a modest increase in elevation and vegetation density as one moves eastward; therefore, Botswana's tableland slopes gently from east to west.

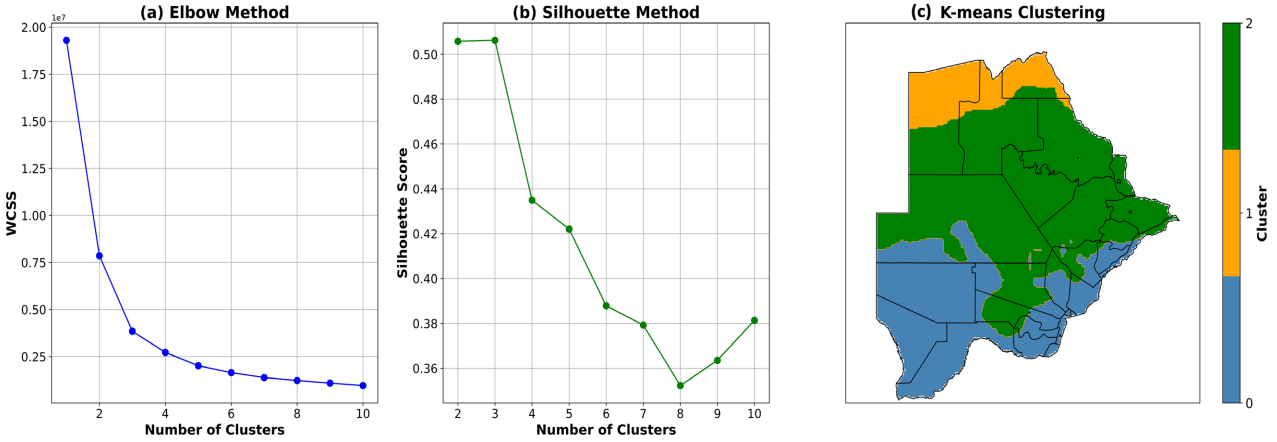

Figure 12. (a) Elbow method, (b) Silhouette method, and (c) resultant k-means clusters.

After the region division or spatial decomposition, we use Ensemble Empirical Mode Decomposition (EEMD) to conduct the temporal decomposition to analyze solar irradiance across different regions at different time scales, as was utilized by (Du et al., 2023). This technique decomposed solar irradiance in Region 1 into three Intrinsic Mode Functions (IMFs) with a dominant period of 3, 8, and 14 years and a residual component that reflects the nonlinear trend. For Region 2, two IMFs with a dominant period of 4 and 10 years are obtained. For Region 3, three IMFs with a dominant period of 3, 6, and 16 years are obtained. Therefore, solar irradiance in all regions exhibits interannual and decadal variations, besides the long-term trends. After decomposing the TCC, HLC, MLC, and LLC averaged over each region by the EEMD method, we examined their correlations with solar irradiance, as displayed in **Figure 13**. First, **Figure 13(a)**, **Figure 13(e)**, and **Figure**

13(i) show that negative correlations between SIR and TCC in all three regions are below −0.9, and the negative correlations are most extensive between SIR and MLC. This confirms the close relationship between the long-term decrease in the mid-level clouds and the increase in the solar irradiance in spring, as illustrated by Figure 6 and Figure 8.

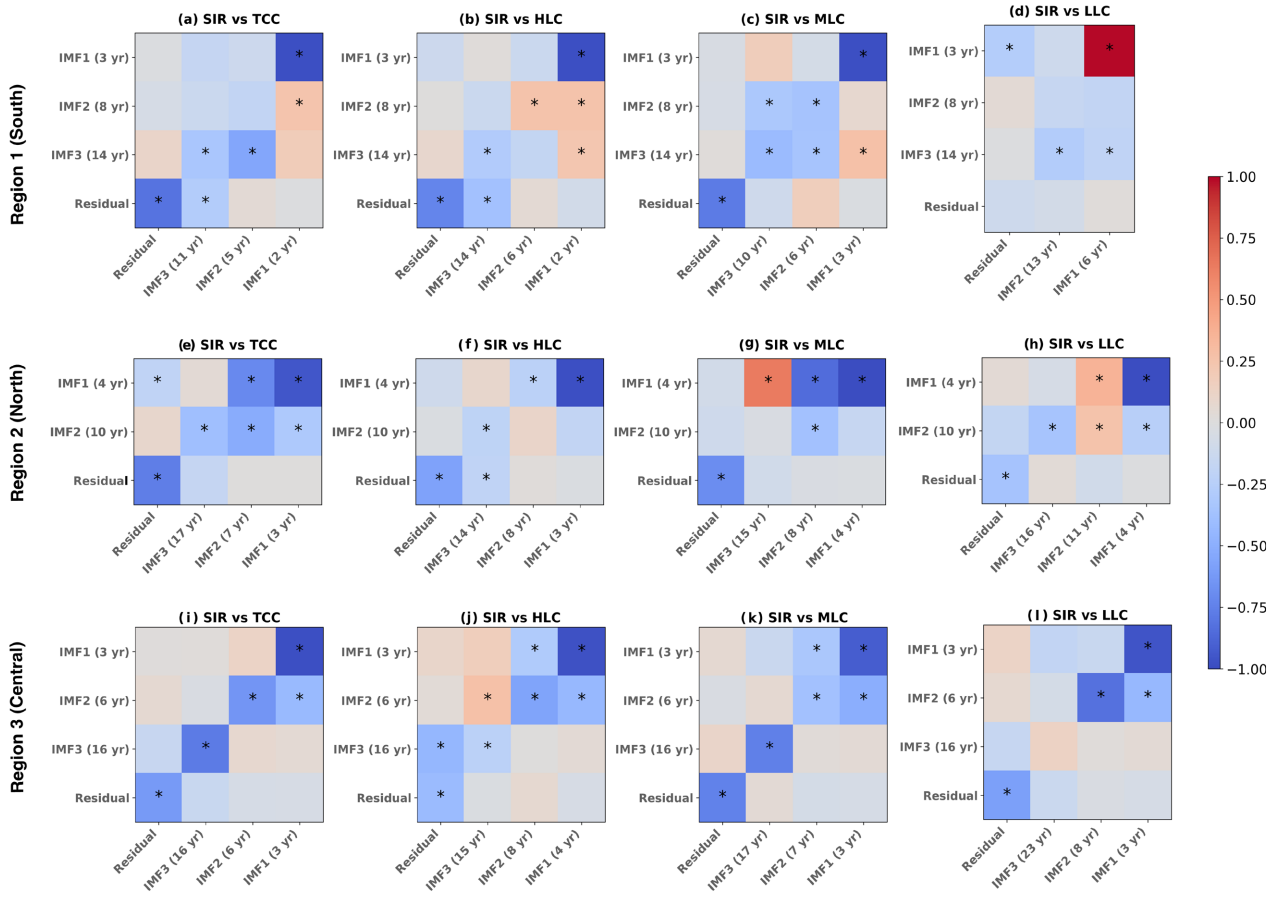

Figure 13. (a)-(l) Correlation coefficients were calculated to analyze the relationship between the intrinsic mode functions (IMFs) and residual components of Botswana's solar irradiance and the IMFs of various cloud levels across the three regional divisions from 1971 to 2020. The asterisks indicate correlation at a 95% statistical confidence interval, as determined by the two-sided Student's t-test. The numbers in parentheses indicate the dominant period of the IMFs.

As to the interannual timescales (IMF1s), it is seen that for all three regions, there is a strong negative correlation of about −0.96 between the SIR and the TCC, HLC, and MLC. While negative correlations are also found between SIR and the LLC in Regions 2 and 3, Region 1 (South) shows a significant positive correlation, suggesting the variable role of LLC across different regions of Botswana. The negative correlation coefficients decreased as the period of IMFs increased to decadal and interdecadal timescales (IMF2s and IMF3s), showing a weaker relationship. For Region 2 (North), the IMF2 of LLC exhibits a positive correlation with the IMF2 of SIR, while they are highly negatively correlated for Region 3 (Central).

Among the three regions, Region 3 shows the most consistent and close inverse

relationship between SIR and TCC across all timescales, where the low-level and mid-level clouds play an essential role for IMF2 and IMF3, respectively. Among different levels, the mid-level clouds show the most stable relationship with the SIR across all timescales, manifested by the negative correlations below −0.92. This suggests that the mid-level clouds can be considered a universally influencing indicator for the solar irradiance forecasts in Botswana. These results not only confirm that clouds play a significant role in the reception of solar irradiance received at the surface, as previously mentioned by Pfister et al. (2003) and Calbo et al. (2005), but also highlight the most various role of low-level clouds in influencing the solar irradiance across different regions in Botswana and across various timescales.

4. Conclusion

The first comprehensive assessment of solar irradiance variability in Botswana over 50 years using ERA5 reanalysis data provides valuable insights for development and policy formulation in the region for solar energy. We show that peak monthly solar irradiance occurs in Botswana during the summer/rainfall season (November-March) at values between 313 and 445 $W \cdot m^{-2}$ for the country. Such areas for these projects are identified, such as the Kalahari Desert and Makgadikgadi Pans, and potential large-sized solar installations are there. Long-term trend analysis indicated that the spring (August-October) constantly increased Botswana's solar irradiance, while a decreasing trend was observed in December solar irradiance, suggesting a seasonal shift in solar resources. This shift could have significant ramifications for the planning and development of a solar energy infrastructure by necessitating modifications in the design and operation of solar power systems to maximize energy capture up and down the year.

In this work, we further investigated the factors influencing solar irradiance variability. Mid-level clouds significantly influence longer-term trends and year-to-year variability in Botswana's solar irradiance than aerosol optical depth. This finding highlights the need to incorporate cloud-associated weather patterns into solar energy planning and forecasting models to improve their accuracy and reliability. Three distinct regions with similar solar irradiance characteristics were identified by K-means clustering, which is a basis for the targeted solar energy development strategies on the country scale. At each identified region, EEMD analysis revealed the link between solar irradiance and cloud cover at different timescales, indicating that atmospheric conditions interact with the potential solar energy in a nonlinear and complex manner. In addition, the aerosols, particularly the sulfate aerosol optical depth in the dry/winter season, exhibit a reverse relationship with the solar irradiance in parts of regions in Botswana, playing a secondary role.

Of particular note, however, the overhead study of the yearly mean solar irradiance averaged over Botswana did not show a significant upward trend in the yearly mean solar irradiance throughout the study period. The stability of long-

term solar resources suggests that Botswana's solar energy potential is robust to short-term variations and seasonal shifts. Although lower climatological means, we observed higher solar irradiance variability in January and February than in other summer months. More sophisticated forecasting and energy management systems would be required to handle the increased variability during these months. This evidence, combined with aerosols' significant impact on Botswana's solar radiance, argues that the impacts of air quality issues on the potential for solar energy development in the region are likely to be minor. Aerosol levels are to be kept under observation to account for any future changes in air quality when planning for solar energy. Our findings significantly contribute to knowledge of solar irradiance variability in Botswana and provide a good base for further research and future developments in solar energy in the region. Policy decisions and investment strategies in the renewable energy sector can be informed by identifying prime locations for solar energy projects and insights into seasonal shifts and regional characteristics. It should be investigated further how the observed seasonal variations in solar resources are caused and how solar irradiance patterns in Botswana might change due to a changing climate. Finally, pairing these results with socio-economic factors and consideration for grid infrastructure can further enhance the prescriptive value of the research and help drive Botswana on its path to a more sustainable energy future.

Acknowledgements

The first author appreciates acknowledging the European Center for Medium Range Forecasting Climate Data Store-Copernicus, the UK Met Office, and the Botswana Meteorological Services for making the data available. Many thanks also to Prof. Yue Yue Yu for supervising and guiding this research.

Conflicts of Interest

The authors declare no conflict of interest regarding the publication of this paper.

References

Ahamed, R., & Alam, W. (2022). Documenting Monthly Climatological Mean of Wave Parameters in the Northern Bay of Bengal Using 40 Years of ECMWF Reanalysis V5 (ERA5) Data. *Thalassas: An International Journal of Marine Sciences, 38,* 71-86. https://doi.org/10.1007/s41208-021-00385-2

Bansal, S. (2019). Application of K-Means Clustering for Designing Power Distribution Network. *Asian Journal of Electrical Sciences, 8,* 11-15. https://doi.org/10.51983/ajes-2019.8.2.2365

Batisani, N., & Yarnal, B. (2010). Rainfall Variability and Trends in Semi-Arid Botswana: Implications for Climate Change Adaptation Policy. *Applied Geography, 30,* 483-489. https://doi.org/10.1016/j.apgeog.2009.10.007

Bhayo, B. A., Al-Kayiem, H. H., Gilani, S. I. U., & Ismail, F. B. (2020). Power Management Optimization of Hybrid Solar Photovoltaic-Battery Integrated with Pumped-Hydro-Storage System for Standalone Electricity Generation. *Energy Conversion and Management,*

215, Article ID: 112942. https://doi.org/10.1016/j.enconman.2020.112942

Bostan, I., Gheorghe, A. V., Dulgheru, V., Bostan, V., Sochireanu, A., & Dicusară, I. (2011). Conversion of Renewable Kinetic Energy of Water: Synthesis, Theoretical Modeling, and Experimental Evaluation. In A. Gheorghe, & L. Muresan (Eds.), *Energy Security* (pp. 125-176). Springer. https://doi.org/10.1007/978-94-007-0719-1_10

BPC Annual Report 2021, Moving towards a Sustainable Future (2021). Botswana Power Corporation. https://www.bpc.bw/about-bpc/annual-reports

Bright, R. M., & O'Halloran, T. L. (2019). Developing a Monthly Radiative Kernel for Surface Albedo Change from Satellite Climatologies of Earth's Shortwave Radiation Budget: CACK V1.0. *Geoscientific Model Development, 12,* 3975-3990. https://doi.org/10.5194/gmd-12-3975-2019

Byakatonda, J., Parida, B. P., Kenabatho, P. K., & Moalafhi, D. B. (2018). Analysis of Rainfall and Temperature Time Series to Detect Long-Term Climatic Trends and Variability over Semi-Arid Botswana. *Journal of Earth System Science, 127,* Article No. 25. https://doi.org/10.1007/s12040-018-0926-3

Calbó, J., Pagès, D., & González, J. (2005). Empirical Studies of Cloud Effects on UV Radiation: A Review. *Reviews of Geophysics, 43,* 1-28. https://doi.org/10.1029/2004rg000155

Charlson, R. J., Schwartz, S. E., Hales, J. M., Cess, R. D., Coakley, J. A., Hansen, J. E. et al. (1992). Climate Forcing by Anthropogenic Aerosols. *Science, 255,* 423-430. https://doi.org/10.1126/science.255.5043.423

Du, Y., Zhang, K., Shao, Q., & Chen, Z. (2023). A Short-Term Prediction Model of Wind Power with Outliers: An Integration of Long Short-Term Memory, Ensemble Empirical Mode Decomposition, and Sample Entropy. *Sustainability, 15,* Article No. 6285. https://doi.org/10.3390/su15076285

Duffie, J. A., & Beckman, W. A. (2013). *Solar Engineering of Thermal Processes*. Wiley. https://doi.org/10.1002/9781118671603

Eckardt, F. D., Bryant, R. G., McCulloch, G., Spiro, B., & Wood, W. W. (2008). The Hydrochemistry of a Semi-Arid Pan Basin Case Study: Sua Pan, Makgadikgadi, Botswana. *Applied Geochemistry, 23,* 1563-1580. https://doi.org/10.1016/j.apgeochem.2007.12.033

Edwards, A. W. F., Cavalli-Sforza, L. L., & Edwards, A. W. F. (1965). *This Content Downloaded from 66.77.17.54 on Sun* (Vol. 21, Issue 2).

Fu, W., Yue, X., Li, Z., Tian, C., Zhou, H., Li, K. et al. (2022). Decoupling between $PM_{2.5}$ Concentrations and Aerosol Optical Depth at Ground Stations in China. *Frontiers in Environmental Science, 10,* Article ID: 979918. https://doi.org/10.3389/fenvs.2022.979918

Gaci, S. (2016). A New Ensemble Empirical Mode Decomposition (EEMD) Denoising Method for Seismic Signals. *Energy Procedia, 97,* 84-91. https://doi.org/10.1016/j.egypro.2016.10.026

Hersbach, H., Bell, B., Berrisford, P., Hirahara, S., Horányi, A., Muñoz-Sabater, J. et al. (2020). The ERA5 Global Reanalysis. *Quarterly Journal of the Royal Meteorological Society, 146,* 1999-2049. https://doi.org/10.1002/qj.3803

Hogan, R. (2015). *Radiation Quantities in the ECMWF Model and MARS*. ECMWF. https://www.sciencemag.org

Huang, N. E., Shen, Z., Long, S. R., Wu, M. C., Shih, H. H., Zheng, Q. et al. (1998). The Empirical Mode Decomposition and the Hilbert Spectrum for Nonlinear and Non-Stationary Time Series Analysis. *Proceedings of the Royal Society of London. Series A:*

Mathematical, Physical and Engineering Sciences, 454, 903-995. https://doi.org/10.1098/rspa.1998.0193

Jacobson, M. Z., & Jadhav, V. (2018). World Estimates of PV Optimal Tilt Angles and Ratios of Sunlight Incident Upon Tilted and Tracked PV Panels Relative to Horizontal Panels. *Solar Energy, 169,* 55-66. https://doi.org/10.1016/j.solener.2018.04.030

Kalogirou, S. A. (2009). Photovoltaic Systems. In S. A. Kalogirou (Ed.), *Solar Energy Engineering* (pp. 469-519). Elsevier. https://doi.org/10.1016/b978-0-12-374501-9.00009-1

Kenabatho, P. K., Parida, B. P., & Moalafhi, D. B. (2012). The Value of Large-Scale Climate Variables in Climate Change Assessment: The Case of Botswana's Rainfall. *Physics and Chemistry of the Earth, Parts A/B/C, 50,* 64-71. https://doi.org/10.1016/j.pce.2012.08.006

Kendall, M. G. (1975). *Rank Correlation Methods* (4th Ed.). Charles Grifin.

Klein, S. A. (1977). Calculation of Monthly Average Insolation on Tilted Surfaces. *Solar Energy, 19,* 325-329. https://doi.org/10.1016/0038-092x(77)90001-9

Lassman, W., Pierce, J. R., Bangs, E. J., Sullivan, A. P., Ford, B., Mengistu Tsidu, G. et al. (2020). Using Low-Cost Measurement Systems to Investigate Air Quality: A Case Study in Palapye, Botswana. *Atmosphere, 11,* Article No. 583. https://doi.org/10.3390/atmos11060583

Levy, H., Horowitz, L. W., Schwarzkopf, M. D., Ming, Y., Golaz, J., Naik, V. et al. (2013). The Roles of Aerosol Direct and Indirect Effects in Past and Future Climate Change. *Journal of Geophysical Research: Atmospheres, 118,* 4521-4532. https://doi.org/10.1002/jgrd.50192

Liu, B. Y. H., & Jordan, R. C. (1960). The Interrelationship and Characteristic Distribution of Direct, Diffuse and Total Solar Radiation. *Solar Energy, 4,* 1-19. https://doi.org/10.1016/0038-092x(60)90062-1

Liu, Y., Jia, R., Dai, T., Xie, Y., & Shi, G. (2014). A Review of Aerosol Optical Properties and Radiative Effects. *Journal of Meteorological Research, 28,* 1003-1028. https://doi.org/10.1007/s13351-014-4045-z

Ma, J., Luo, Y., Shen, Y., Liang, H., & Li, S. (2013). Regional Long-Term Trend of Ground Solar Radiation in China over the Past 50 Years. *Science China Earth Sciences, 56,* 1242-1253. https://doi.org/10.1007/s11430-012-4419-y

Mann, H. B. (1945). Nonparametric Tests against Trend. *Econometrica, 13,* Article No. 245. https://doi.org/10.2307/1907187

Mucomole, F. V., Silva, C. A. S., & Magaia, L. L. (2023). Temporal Variability of Solar Energy Availability in the Conditions of the Southern Region of Mozambique. *American Journal of Energy and Natural Resources, 2,* 27-50. https://doi.org/10.54536/ajenr.v2i1.1311

Mühlemann, D., Folini, D., Pfenninger, S., Wild, M., & Wohland, J. (2022). Meteorologically-Informed Spatial Planning of European PV Deployment to Reduce Multiday Generation Variability. *Earth's Future, 10,* e2022EF002673. https://doi.org/10.1029/2022ef002673

Ndabagenga, D. M., Yu, J., Mbawala, J. R., Ntigwaza, C. Y., & Juma, A. S. (2023). Climatic Indices' Analysis on Extreme Precipitation for Tanzania Synoptic Stations. *Journal of Geoscience and Environment Protection, 11,* 182-208. https://doi.org/10.4236/gep.2023.1112010

Nijegorodov, N., Luhanga, P. V. C., & King, J. G. (2005). Comprehensive Experimental and Theoretical Investigation of Solar Radiation Conditions in Botswana: A Semi-Desert Region. *International Energy Journal, 6,* 1-12. https://www.serd.ait.ac.th/reric

Okakwu, I. K., Olabode, O. E., Ade-Ikuesan, O. O., Airoboman, A. E. (2019). Sizing an Off-Grid Photovoltaic System and Economic Comparison with Petrol Generator Using Life Cycle Cost (LCC) Approach for a Typical Rural Primary Healthcare Center in Nigeria. *Journal of Energy and Safety Technology (JEST), 2,* 41-47. https://doi.org/10.11113/jest.v2n2.45

Pfister, G., McKenzie, R. L., Liley, J. B., Thomas, A., Forgan, B. W., & Long, C. N. (2003). Cloud Coverage Based on All-Sky Imaging and Its Impact on Surface Solar Irradiance. *Journal of Applied Meteorology, 42,* 1421-1434. https://doi.org/10.1175/1520-0450(2003)042<1421:ccboai>2.0.co;2

Ramanathan, V., Crutzen, P. J., Kiehl, J. T., & Rosenfeld, D. (2001). Aerosols, Climate, and the Hydrological Cycle. *Science, 294,* 2119-2124. https://doi.org/10.1126/science.1064034

Sarbu, I., & Sebarchievici, C. (2017). Solar Radiation. In I. Sarbu, & C. Sebarchievici (Eds.), *Solar Heating and Cooling Systems* (pp. 13-28). Elsevier. https://doi.org/10.1016/b978-0-12-811662-3.00002-5

Sen, P. K. (1968). Estimates of the Regression Coefficient Based on Kendall's Tau. *Journal of the American Statistical Association, 63,* 1379-1389. https://doi.org/10.1080/01621459.1968.10480934

Shahapure, K. R., & Nicholas, C. (2020). Cluster Quality Analysis Using Silhouette Score. In *2020 IEEE 7th International Conference on Data Science and Advanced Analytics (DSAA)* (pp. 747-748). IEEE. https://doi.org/10.1109/dsaa49011.2020.00096

Shekata, G. D., Tibba, G. S., & Baheta, A. T. (2024). CFD Simulation of a Solar Collector Integrated with PCM Thermal Storage. *Energy Storage, 6,* e592. https://doi.org/10.1002/est2.592

SKR Engineering College, Institute of Electrical and Electronics Engineers, Madras Section, & Institute of Electrical and Electronics Engineers (2017). *International Conference on Energy, Communication, Data Analytics & Soft Computing (ICECDS).*

Stephenson, D. G. (1967). *Tables of Solar Altitude and Azimuth; Intensity and Solar Heat Gain Tables.* Technical Paper 243, National Research Council of Canada. https://doi.org/10.4224/20378809

Streiner, D. L. (1996). Maintaining Standards: Differences between the Standard Deviation and Standard Error, and When to Use Each. *The Canadian Journal of Psychiatry, 41,* 498-502. https://doi.org/10.1177/070674379604100805

Takemura, T., Nozawa, T., Emori, S., Nakajima, T. Y., & Nakajima, T. (2005). Simulation of Climate Response to Aerosol Direct and Indirect Effects with Aerosol Transport-radiation Model. *Journal of Geophysical Research: Atmospheres, 110,* D02202. https://doi.org/10.1029/2004jd005029

Tlhalerwa, K., & Mulalu, M. (2019). Assessment of the Concentrated Solar Power Potential in Botswana. *Renewable and Sustainable Energy Reviews, 109,* 294-306. https://doi.org/10.1016/j.rser.2019.04.019

Umargono, E., Suseno, J. E., & Gunawan, V. (2020). K-means Clustering Optimization Using the Elbow Method and Early Centroid Determination Based-On Mean and Median Formula. In *Proceedings of the International Conferences on Information System and Technology* (pp. 121-129). Atlantis Press. https://doi.org/10.5220/0009908402340240

Voigt, A., Albern, N., Ceppi, P., Grise, K., Li, Y., & Medeiros, B. (2020). Clouds, Radiation, and Atmospheric Circulation in the Present-Day Climate and under Climate Change. *WIREs Climate Change, 12,* e694. https://doi.org/10.1002/wcc.694

Yahyaoui, Z., Hajji, M., Mansouri, M., & Bouzrara, K. (2023). One-Class Machine Learning

Classifiers-Based Multivariate Feature Extraction for Grid-Connected PV Systems Monitoring under Irradiance Variations. *Sustainability, 15,* Article No. 13758. https://doi.org/10.3390/su151813758

Yue, S., & Wang, C. (2004). The Mann-Kendall Test Modified by Effective Sample Size to Detect Trend in Serially Correlated Hydrological Series. *Water Resources Management, 18,* 201-218. https://doi.org/10.1023/b:warm.0000043140.61082.60

Supplementary Material

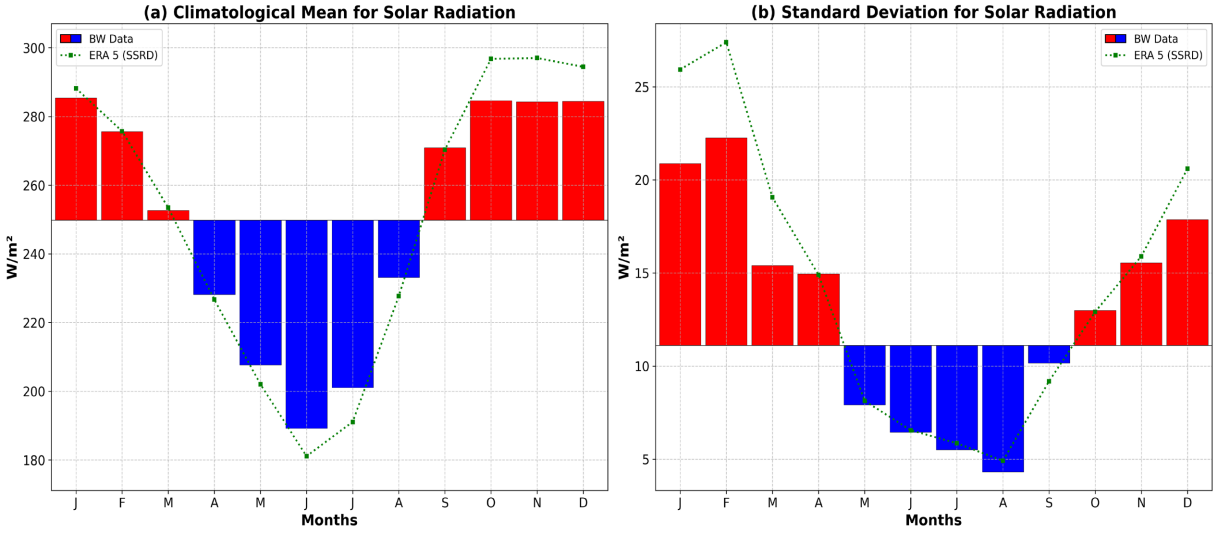

Figure S1. Comparison of solar radiation data between BW Data (bars) and ERA 5 SSRD (green dashed line) for 1983-2015. (a) Climatological Mean for Solar Radiation: The mean solar radiation in watts per square meter (W/m^2) is plotted for each month. Red bars represent positive deviations from the annual mean, while blue bars represent negative deviations. The green dashed line shows the corresponding ERA 5 SSRD values. (b) Standard Deviation for Solar Radiation: The standard deviation of monthly solar radiation indicates variability. Red bars represent positive values, blue bars show negative values, and the green dashed line represents ERA 5 SSRD variability.

Further comparison denoted in Supplementary **Figure S1** compares solar radiation data from 1983-2015 from BW Data (bars) and ERA 5 SSRD (Surface Solar Radiation Downward, the green dashed line). The left subplot (a) shows a climatological mean of solar radiation. In contrast, in the right subplot (b), the standard deviation of solar radiation is given for the monthly periods. The climatological mean plot shows extreme seasonality in solar radiation. The BW Data can be read as differences in solar radiation levels throughout the years, as the red bars represent positive values and the blue bars represent negative values. In particular, solar radiation values are highest in the summer months (in December, January, and February), reaching around 282 W/m^2 in January for BW Data. This follows a gradual decline towards March. Significant lower values are observed between winter months (May to July), with a minimum in June and July under 200 W/m^2. Blue bars represent this seasonal dip in deviations from the annual mean. ERA 5 SSRD data exhibit similar seasonal patterns but are higher than the BW Data in most months. This discrepancy is particularly conspicuous in winter, when ERA 5 SSRD tops at 181 W/m^2, while BW Data lags. Either data collection methodologies or spatial resolution differences could explain the discrepancy between BW Data and ERA 5 SSRD. Meanwhile, the BW Data may locally represent localized measurements that feature local characteristics, and ERA 5 SSRD is a broader reanalysis dataset with global coverage.

The solar radiation across different months is shown in the variability of a standard deviation plot. Similar to the climatological mean, there is a marked

seasonal trend: For both BW Data and ERA 5 SSRD, standard deviations are more significant in summer, reaching above 25 W/m^2 in January and December. This means that there is higher solar radiation variability during these months. Standard deviations, though, are much more minor during winter, below 10 W/m^2 for both datasets in May, June, July, and August. This means this period is more stable for solar radiation. In terms of winter versus summer, ERA 5 SSRD data are found to be generally less (more) variable than that from BW Data. Thus, ERA 5 SSRD may pick up on broader scale variations that are less clear in the localized BW Data.

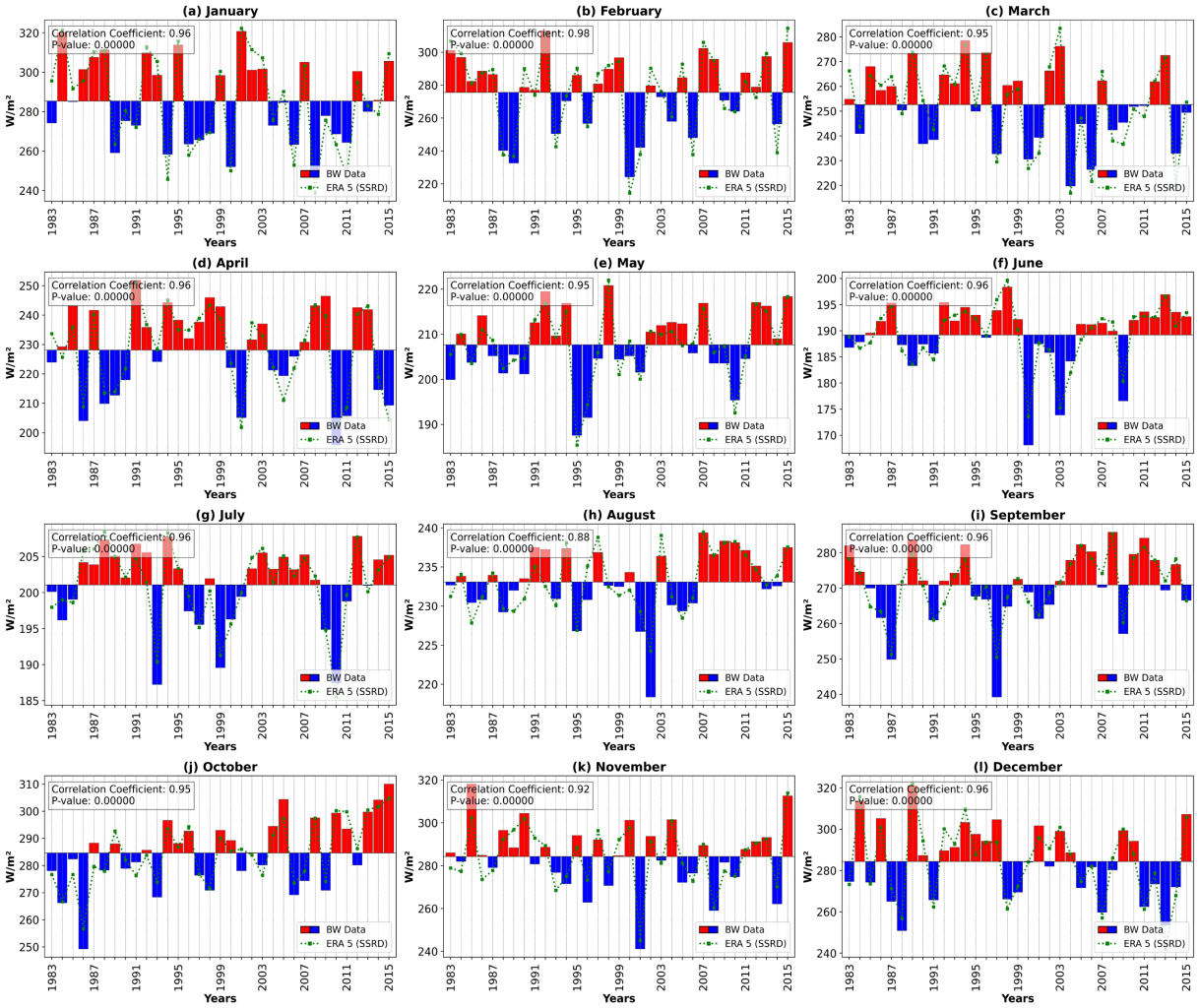

Figure S2. Timeseries interannual solar radiation variability for each month from January to December from 1983 to 2015. The red bars represent deviations in BW Data (W/m^2), while the blue bars represent negative deviations. The green dashed line corresponds to ERA 5 SSRD values (W/m^2). Each subplot includes the correlation coefficient and p-value, indicating the strength and statistical significance at a 95% confidence interval of the relationship between BW Data and ERA 5 SSRD. The high correlation coefficients (ranging from 0.88 to 0.98) suggest a strong agreement between the two datasets, with statistically significant p-values ($p < 0.00001$) across all months.

Still, from 1983 to 2015, BW Data and ERA 5 SSRD were further compared in Supplementary **Figure S2** on monthly trends and interannual variability. With these Figures, we can explore more closely the correlation between the two

datasets on a month-to-month and a year-to-year basis. Each month shows the correlation coefficient and p-value for the interannual solar radiation variability from January through December. A consistently high correlation coefficient (average 0.88 to 0.98) between BW Data and ERA 5 SSRD demonstrated a robust positive relationship for all months. This implies that both sets of datasets reflect similar long-term trends in solar radiation. These correlations are statistically significant as the p-values are low ($p < 0.00001$). The data shows a clear seasonal pattern: The highest mean solar radiation values are exhibited during the summer months (December to February), with the highest peak between December and January (320 W/m^2). The same trend is seen in both datasets, with BW Data reporting slightly less than ERA 5 SSRD. Low solar radiation values are shown during winter (May to July), with minimums around June and July (~205 W/m^2). ERA 5 SSRD, as with BW Data again, reports higher values than advertised. There is a shift from winter to summer, and solar radiation values rise (Spring: August). Indeed, these monthly plots also reveal periods of more substantial interannual variability, perhaps a consequence of more variable weather conditions during these periods, with solar radiation levels more affected by these.

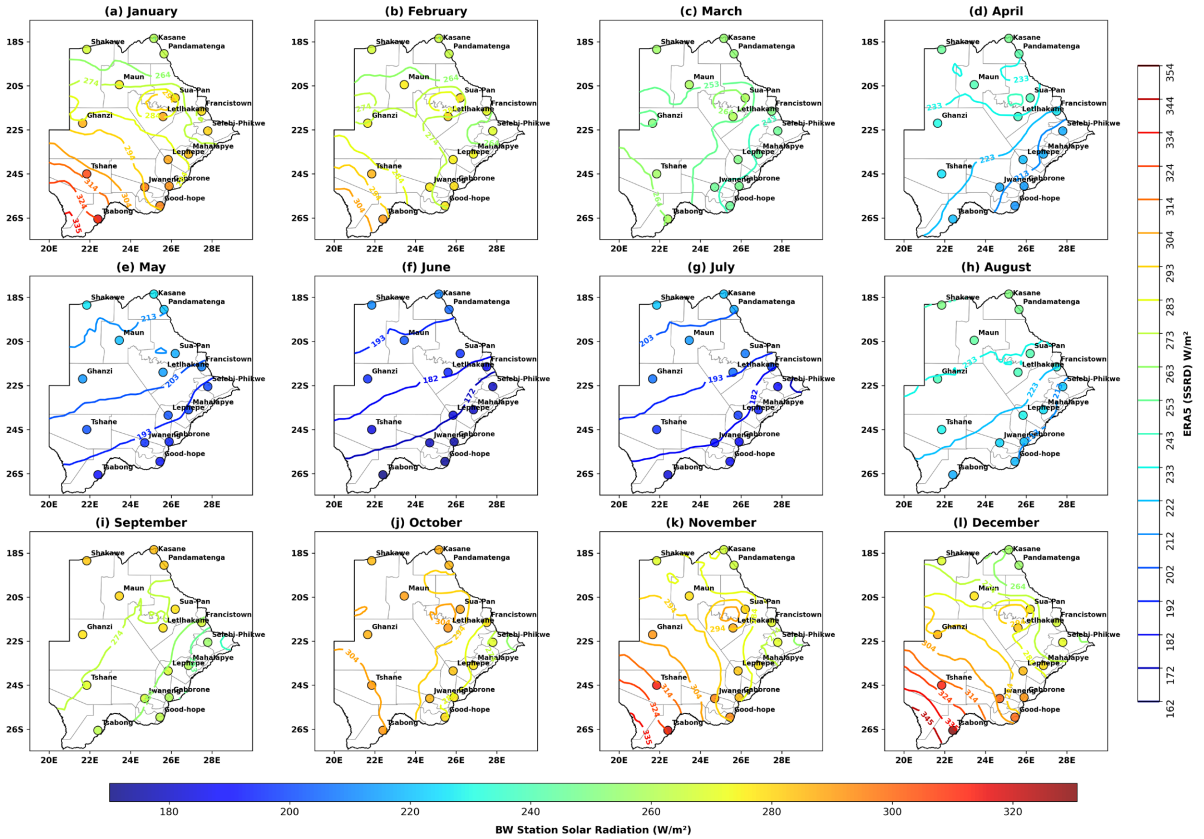

Figure S3. Spatial climatologies of solar radiation across Botswana for each month from January to December from 1983 to 2015. The color contour maps represent ERA 5 SSRD data (W/m^2), while the colored circles at station locations depict BW Data in W/m^2. Sub-plots (a-l): Monthly spatial distribution of solar radiation, with warmer colors indicating higher values and cooler colors representing lower values. The southern regions generally exhibit higher solar radiation than the northern areas, particularly during summer (December to February).

Supplementary Figure S3 shows spatial climatologies of solar radiation against different stations in Botswana at a monthly scale. The color contours represent the ERA 5 SSRD values. In contrast, the circles at station locations represent BW Data values. The highest solar radiation values occur during summer (December to February) across most stations, with December achieving peaks at 280 - 320 W/m^2. Values at the southern stations are greater than those measured at the northern stations (e.g., Tsab-ong, Tshane vs Kasane, Pandamatenga). Significant reduction in solar radiation is also observed during winter (May to July), with June and July at a minimum of 180 - 220 W/m^2. Despite some differences in the values, ERA 5 sees a higher (but the same) value than BW Data; the pattern is consistent. Along with all stations, solar radiation values increase in spring (August), transitioning from winter to summer. Spatial patterns indicate that solar radiation to southern stations exceeds that to northern stations during the period considered. However, it might be explained by latitudinal differences or regional climatic factors. Generally, the agreement between BW Data and ERA 5 SSRD is good, with some discrepancies in magnitude, especially during the summer months.

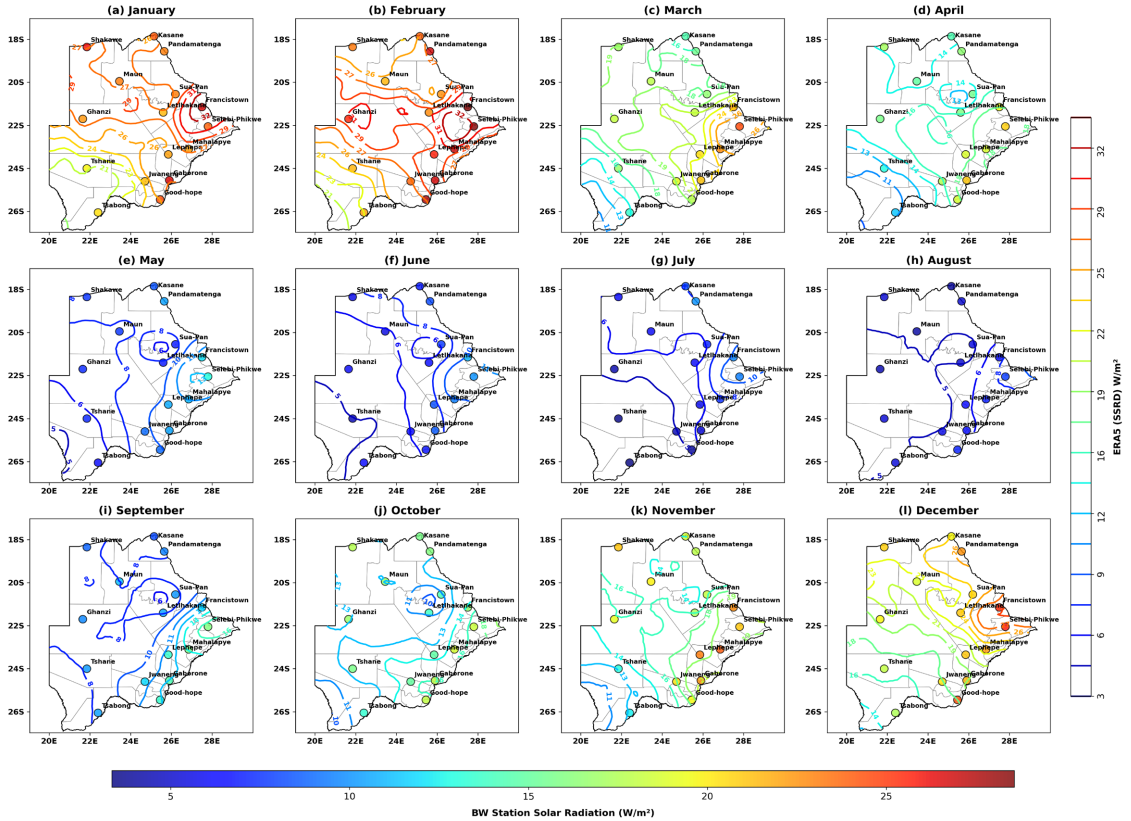

Figure S4. Spatial standard deviations of solar radiation across Botswana for each month from January to December from 1983 to 2015. The color contours represent the standard deviation of ERA 5 SSRD data (W/m^2), while the colored circles at station locations depict the standard deviation of BW Data in W/m^2. Sub-plots (a-l): Monthly spatial distribution of solar radiation variability, with warmer colors indicating higher variability and cooler colors representing lower variability. The highest variability is observed during the summer months (December to February), particularly in the northern to eastern regions, while winter months (May to July) show more stable solar radiation with lower variability across all areas.

Supplementary **Figure S4** presents the spatial distribution of the standard deviation of solar radiation for each month, indicating variability: The variability in summer months (December and January to February) is greater than the other months and suggests that standard deviations are 25 - 32 W/m^2 in northern to eastern regions. This means there are more solar radiation fluctuations during these months, most likely caused by more turbulent weather or cloud cover variation. Conversely, variability during the winter (May to July) is much lower, with 6 - 15 W/m^2 standard deviations in almost all regions. This was during a more stable level of solar radiation. Standard deviations are significant during transition months (March-April and August-September), similar to summer variability. Spatial patterns of standard deviation are consistent between BW Data and ERA 5 SSRD, but those standard deviations of the latter are slightly higher over some areas. It may indicate that ERA 5 better reveals larger-scale atmospheric processes that local station observations may not fully represent.